

Proton-Detected Solid-State NMR Spectroscopy of Spin-1/2 Nuclei with Large Chemical Shift Anisotropy

Amrit Venkatesh,^{1,2} Frédéric A. Perras,¹ Aaron J. Rossini^{1,2}*

¹US DOE Ames Laboratory, Ames, Iowa, USA, 50011

²Iowa State University, Department of Chemistry, Ames, IA, USA, 50011

Corresponding Author

*e-mail: arossini@iastate.edu

ABSTRACT

Constant-time (CT) dipolar heteronuclear multiple quantum coherence (D-HMQC) has previously been demonstrated as a method for proton detection of high-resolution wide-line NMR spectra of spin-1/2 nuclei with large chemical shift anisotropy (CSA). However, ^1H transverse relaxation and t_1 -noise often reduce the sensitivity of D-HMQC experiments, preventing the theoretical gains in sensitivity provided by ^1H detection from being realized. Here we demonstrate a series of improved pulse sequences for ^1H detection of spin-1/2 nuclei under fast MAS, with ^{195}Pt SSNMR experiments on cisplatin as an example. First, a new t_1 -incrementation protocol for D-HMQC dubbed Arbitrary Indirect Dwell (AID) is demonstrated. AID allows the use of arbitrary, rotor asynchronous t_1 -increments, but removes the constant time period from CT D-HMQC, resulting in improved sensitivity by reducing transverse relaxation losses. Next, we show that short high-power adiabatic pulses (SHAPs), which efficiently invert broad MAS sideband manifolds, can be effectively incorporated into ^1H detected symmetry-based resonance echo double resonance (S-REDOR) and t_1 -noise eliminated D-HMQC experiments. The S-REDOR experiments with SHAPs provide approximately double the dipolar dephasing, as compared to experiments with rectangular inversion pulses. We lastly show that sensitivity and resolution can be further enhanced with the use of swept excitation pulses as well as adiabatic magic angle turning.

Introduction

The solid-state NMR spectra of many elements are often severely broadened by chemical shift anisotropy (CSA) or the second-order quadrupolar interaction.¹⁻³ Heavy spin-1/2 nuclei such as ¹¹⁹Sn, ¹⁹⁵Pt, ¹⁹⁹Hg, ²⁰⁷Pb, etc. often possess large CSA on the order of thousands of parts per million (ppm), leading to solid-state NMR spectra that are often hundreds of kHz broad. For example, square planar Pt complexes are known to possess ¹⁹⁵Pt CSA in excess of 7000 ppm, leading to ¹⁹⁵Pt static and magic angle spinning (MAS) spectra which often exceed 500 kHz in breadth, even at moderate magnetic fields.⁴⁻⁶ Conventional one-pulse, or spin-echo techniques are often impractical to obtain wide-line solid-state NMR spectra because the available rf fields are often insufficient to uniformly excite broad solid-state NMR powder patterns. One solution to this problem is to use the variable offset cumulative spectroscopy (VOCS) approach to obtain solid-state NMR spectra in a piecewise manner.⁷ Microcoil NMR probes⁸ and frequency-swept pulse sequences have shown to improve excitation bandwidths of 1D spectra.⁹ Schurko and co-workers have developed Wideband Uniform Rate Smooth Truncation (WURST)¹⁰⁻¹¹ - Carr-Purcell Meiboom-Gill (CPMG)¹² or WCPMG that exploits WURST pulses for broadband excitation, and provides a sensitivity gain by detection of an echo train that decays with the refocused homogeneous transverse relaxation time constant (T_2'), in comparison to the decay of a single echo due to inhomogeneous transverse relaxation time constant (T_2^*).¹³ Broadband adiabatic inversion cross polarization (BRAIN-CP) further enhances sensitivity by polarization transfer from nearby high- γ spins such as ¹H;¹⁴ adiabatic inversion sequences have also been used to measure

longitudinal relaxation constants (T_1).¹⁵ BRAIN-CP WCPMG sequences can be implemented into the VOCS procedures to accelerate acquisition times and reduce the number of sub-spectra required. Dynamic nuclear polarization (DNP) has further improved the sensitivity of BRAIN-CP-WCPMG NMR experiments with heavy spin-1/2 nuclei¹⁶⁻¹⁷ and enabled the characterization of low-concentration surface Pt sites in heterogenous catalysts.¹⁸ MAS based experiments have also been used to improve the resolution of overlapping sideband manifolds, for instance by experiments such as magic-angle-turning (MAT)¹⁹⁻²⁰ or PASS-PIETA.²¹ Recently, Altenhof *et al.* demonstrated the use of MAS CPMG experiments for the acquisition of wide-line spectra.²²

Fast MAS (MAS with frequencies > 30 kHz) is a powerful approach to improve the sensitivity and resolution of SSNMR spectra.²³⁻²⁵ Notably, Lange, Nishiyama and coworkers have used fast MAS frequencies of 75 kHz to improve ^{119}Sn SSNMR sensitivity by focusing the intensity of ^{119}Sn CSA patterns into fewer sidebands.²⁶ Fast MAS has been combined with indirect detection to obtain SSNMR spectra of spin-1/2 nuclei such as ^{13}C , ^{15}N , and ^{29}Si using double cross polarization (CP) schemes.²⁷⁻³² However, CP schemes often fail when studying quadrupolar nuclei or spin-1/2 nuclei with large CSA. The indirect detection of half-integer and the spin-1 quadrupolar nucleus ^{14}N has been facilitated by the dipolar heteronuclear multiple quantum coherence (D-HMQC) pulse sequences.³³⁻³⁷ We have previously shown that fast MAS constant-time (CT) D-HMQC can enable the ^1H detection of wide-line ^{195}Pt spectra.³⁸ CT D-HMQC was combined with adiabatic MAT³⁹ to yield high-resolution techniques for the determination of isotropic shifts of overlapping wide-line spectra.⁴⁰ Amoureux and coworkers have investigated various pulse schemes for the excitation of ^{195}Pt signals in D-HMQC sequences; notably, they showed that rotor-synchronized D-HMQC experiments are valuable for the fast determination of isotropic shifts by the acquisition of 2D spectra at two different MAS frequencies.⁴¹⁻⁴²

We recently reported modified pulse sequences to reduce t_1 -noise in 2D ^1H detected D-HMQC spectra with half-integer quadrupolar nuclei and spin-1/2 nuclei, dubbed t_1 -noise eliminated (TONE) D-HMQC.⁴³⁻⁴⁴ The combination of fast MAS $^1\text{H}\{^{195}\text{Pt}\}$ TONE D-HMQC and static DNP enhanced $^1\text{H}\rightarrow^{195}\text{Pt}$ BRAIN-CP-WCPMG was then used to characterize a Pt-based organometallic and single-site silica-supported compound.⁴⁴ Short high-power adiabatic pulses (SHAPs)^{39,45} have been previously incorporated into aMAT D-HMQC,⁴⁰ TONE D-HMQC and S-REDOR (symmetry-based resonance echo double resonance) experiments⁴⁴ on samples with ^{195}Pt CSA (span) of greater than 8000 ppm, however the efficiency of inversion was not systematically investigated. We note that Carvalho and Pell have recently provided an in-depth investigation of the inversion of large CSA sideband manifolds with SHAPs and sideband selective WURST pulses.⁴⁶

Here, we demonstrate a series of modified fast MAS ^1H detected pulse sequences for spin-1/2 nuclei with large CSA, using ^{195}Pt SSNMR experiments on cisplatin as an example. First, a new t_1 -incrementation protocol for CT D-HMQC, dubbed Arbitrary Indirect Dwell (AID), is shown to provide improved sensitivity for indirect detection of wideline SSNMR spectra. Next, we investigate in detail the efficiency of SHAPs to invert a broad ^{195}Pt CSA pattern. We then demonstrate the increased inversion efficiency of SHAPs in comparison to rectangular high-power pulses, in ^1H detected S-REDOR experiments. Modified $^1\text{H}\{^{195}\text{Pt}\}$ D-HMQC and aMAT D-HMQC pulse sequences incorporating the TONE schemes for t_1 -noise elimination are also shown. Finally, the use of swept pulses to improve the excitation efficiency of ^{195}Pt in D-HMQC experiments is explored.

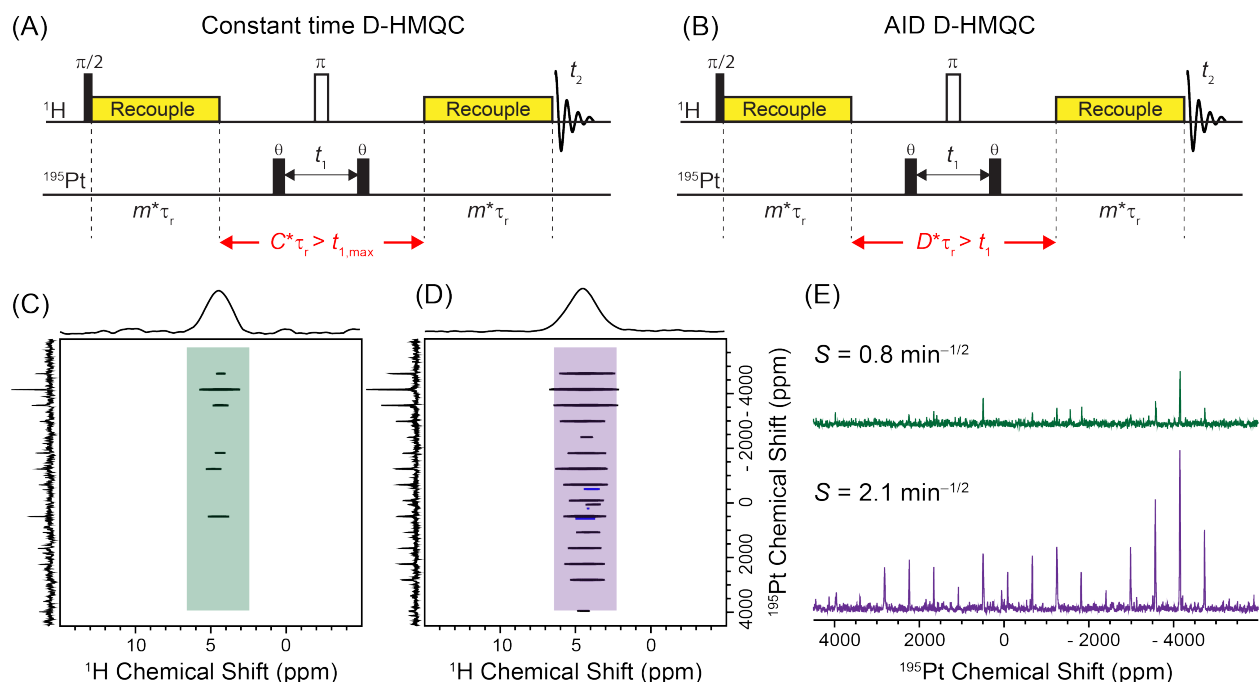


Figure 1. (A) Constant-time (CT) and (B) Arbitrary Indirect Dwell (AID) D-HMQC pulse sequences. 2D $^1\text{H}\{^{195}\text{Pt}\}$ D-HMQC spectra acquired with (C) CT and (D) AID techniques. (E) Comparison of ^{195}Pt traces from 2D spectra shown in (C) and (D). Sensitivity of the ^{195}Pt traces in (E) is calculated based on the signal-to-noise ratio of the most intense sideband at -4153 ppm. 2D spectra shown in (C) and (D) are plotted with the same contour floor level. Spectra were acquired with a 1 s recycle delay, 16 scans, an indirect spectral width of 1 MHz and 2048 t_1 increments. The CT D-HMQC spectrum shown in (C) was obtained with $C = 52$. States-TPPI was used for quadrature in t_1 .

Results and Discussion

Arbitrary Indirect Dwell HMQC. Conventional D-HMQC experiments are performed with rotor-synchronized incrementation of the indirect dimension evolution time (t_1) because when non- γ -encoded recoupling is used to reintroduce the heteronuclear dipolar interactions the rotor must have the same, or inverted, phase at the beginning of the second recoupling block that it did at the beginning of the first block.⁴⁷ In addition, rotor-synchronized incrementation also ensures that the ^1H refocusing pulse falls in between rotor cycles or at half of a rotor cycle; incrementation of t_1 in finer steps will result in appearance of additional spinning sidebands in the indirect dimension that arise from modulation of ^1H CSA and dipolar interactions.⁴⁸ Consequently, the indirect dimension

spectral width (F_1) of conventional D-HMQC spectra is usually limited to the MAS frequency, preventing the acquisition of wide-line MAS solid-state NMR spectra.

The CT D-HMQC pulse sequence incorporates a constant-time, rotor-synchronized spin echo period ($C \times \tau_r$) on the ^1H channel, with the even integer C chosen so that $C \times \tau_r$ is greater than the maximum indirect dimension evolution time ($t_{1,\text{max}}$, Figure 1A).³⁸ CT D-HMQC allows arbitrary t_1 evolution times and spectral widths, and has permitted the acquisition of complete ^{195}Pt sideband manifolds spanning ca. 1 MHz in frequency.³⁸ However, CT D-HMQC experiments are disadvantaged by a significant loss in sensitivity that occurs for all increments of the 2D experiment because of ^1H transverse relaxation during the constant-time period.⁴⁹ Furthermore, the t_1 -noise increases with longer ^1H echo durations due to accumulated rotor synchronization errors. Fast MAS frequencies improve sensitivity by increasing $^1\text{H } T_2'$, however, even at the fastest accessible MAS frequencies, $^1\text{H } T_2'$ are often on the order of 1 ms in protonated, rigid solids.²⁴

Here, the sensitivity of the CT D-HMQC experiments are increased by using a non-uniform incrementation of the ^1H spin echo delay. The proposed experiment is dubbed Arbitrary Indirect Dwell (AID) D-HMQC, and the pulse sequence is shown in Figure 1B. AID D-HMQC combines the advantages of the incremented and CT D-HMQC pulse sequences, i.e., it incorporates an incremented ^1H echo delay while permitting arbitrary, rotor-asynchronous t_1 -increments. The pulse program code of AID D-HMQC is modified to increment the even integer D so that the ^1H echo delay ($D \times \tau_r$) is always greater than t_1 , in contrast to a conventional D-HMQC sequence where the ^1H echo delay is increased by the t_1 -increment or in CT D-HMQC where the echo delay is fixed. Notably an analogous modification was proposed by Lu et al.,⁵⁰ however, here we provide a more detailed investigation of the sensitivity gains and line shape effects with the AID scheme.

Consider a hypothetical AID D-HMQC experiment with an MAS frequency of 50 kHz (20 μ s rotor period), the θ pulses on the X channel are Dirac pulses, and $\Delta t_1 = 1 \mu$ s corresponding to a 1 MHz F_1 spectral width. First, the ^1H echo duration is fixed to 40 μ s ($D = 2$), which will allow up to 39 t_1 -increments (78 t_1 -increments if hyper-complex acquisition is used) to be obtained while always fulfilling the condition $D \times \tau_r > t_1$. At the 40th increment $t_1 = 40 \mu$ s, D is incremented to 4 to satisfy the condition $D \times \tau_r > t_1$ while allowing further t_1 incrementation up to 79 μ s. D is incremented in this fashion until all the t_1 points have been acquired. A video illustrating the differences in t_1 -incrementation between CT and AID D-HMQC is provide as Supporting Information. In practice, implementing the AID protocol into D-HMQC pulse sequences is simple and straightforward; only a few lines of additional code are required to calculate the echo delay as the t_1 -evolution time is incremented (see Bruker pulse programs provided as Supporting Information).

Figure 1C and 1D show 2D $^1\text{H}\{^{195}\text{Pt}\}$ conventional D-HMQC and AID D-HMQC spectra of cisplatin obtained with similar acquisition parameters ($\nu_{\text{rot}} = 50 \text{ kHz}$, $t_{1,\text{max}} = 1024 \mu$ s and 1 MHz F_1 spectral width). The indirect dimension acquisition time necessitates a ^1H echo period of 52 rotor cycles ($C = 52$, $C \times \tau_r = 1040 \mu$ s) with CT D-HMQC, resulting in a 2D spectrum with lower signal-to-noise ratio (SNR, Figure 1C). However, AID D-HMQC allows the acquisition of the same 2D spectrum with enhanced SNR (Figure 1D). The ^{195}Pt slices extracted from the 2D spectra are compared in Figure 1E, where the sensitivity (S), defined as the SNR per square root of unit time, is provided. CT D-HMQC provides a low SNR ^{195}Pt sideband manifold with $S = 0.8 \text{ min}^{-1/2}$ whereas AID D-HMQC shows a higher SNR manifold with $S = 2.1 \text{ min}^{-1/2}$. AID D-HMQC thus provided a factor 2.6 ($2.1 \text{ min}^{-1/2}/0.8 \text{ min}^{-1/2}$) improvement in sensitivity, corresponding to 7-fold savings in experimental time. $^1\text{H}\{^{195}\text{Pt}\}$ 2D spectra acquired with a shorter total evolution time

($t_{1,\max} = 288 \mu\text{s}$) display sensitivities of $2.7 \text{ min}^{-1/2}$ and $3.5 \text{ min}^{-1/2}$ for CT D-HMQC and AID D-HMQC, respectively (Figure S1). In this case the resulting gain in sensitivity with AID D-HMQC is reduced to 1.3 due to reduced ^1H T_2 relaxation losses during the shorter echo duration. Note that the enhanced sensitivity obtained in D-HMQC experiments with the reduced value of $t_{1,\max}$ comes at the cost of a slight loss in ^{195}Pt resolution. Nevertheless, AID D-HMQC will always provide a sensitivity comparable to or higher than CT D-HMQC. The only trade-off of using AID (or a conventional D-HMQC experiment), is that transverse relaxation of the ^1H spin will be encoded on the indirect dimension signal, resulting in reduced resolution in the indirect dimension.⁴⁹ The trade-off between sensitivity and resolution is observed in many constant-time solid-state NMR experiments.⁵¹⁻⁵⁶

To demonstrate that AID D-HMQC is applicable for the indirect detection of a wide range of nuclei, we have performed $^1\text{H}\{^{35}\text{Cl}\}$ population transfer (PT) TONE D-HMQC-3 experiments with L-histidine·HCl·H₂O. The addition of the AID t_1 -incrementation protocol did not introduce distortions in the second-order quadrupolar lineshape and resulted in improved sensitivity as compared to a constant-time experiment (Figure S2). As expected, AID t_1 -incremented and conventional t_1 -incremented D-HMQC spectra are equivalent when a rotor-synchronized t_1 -increment is used. (Figure S3). Therefore, we anticipate that AID D-HMQC will also find utility for the indirect detection of any nucleus that requires indirect dimension spectral widths that exceed the MAS frequency. AID D-HMQC may be particularly beneficial for experiments under slower MAS conditions where the indirect spectral width is limited with conventional D-HMQC.

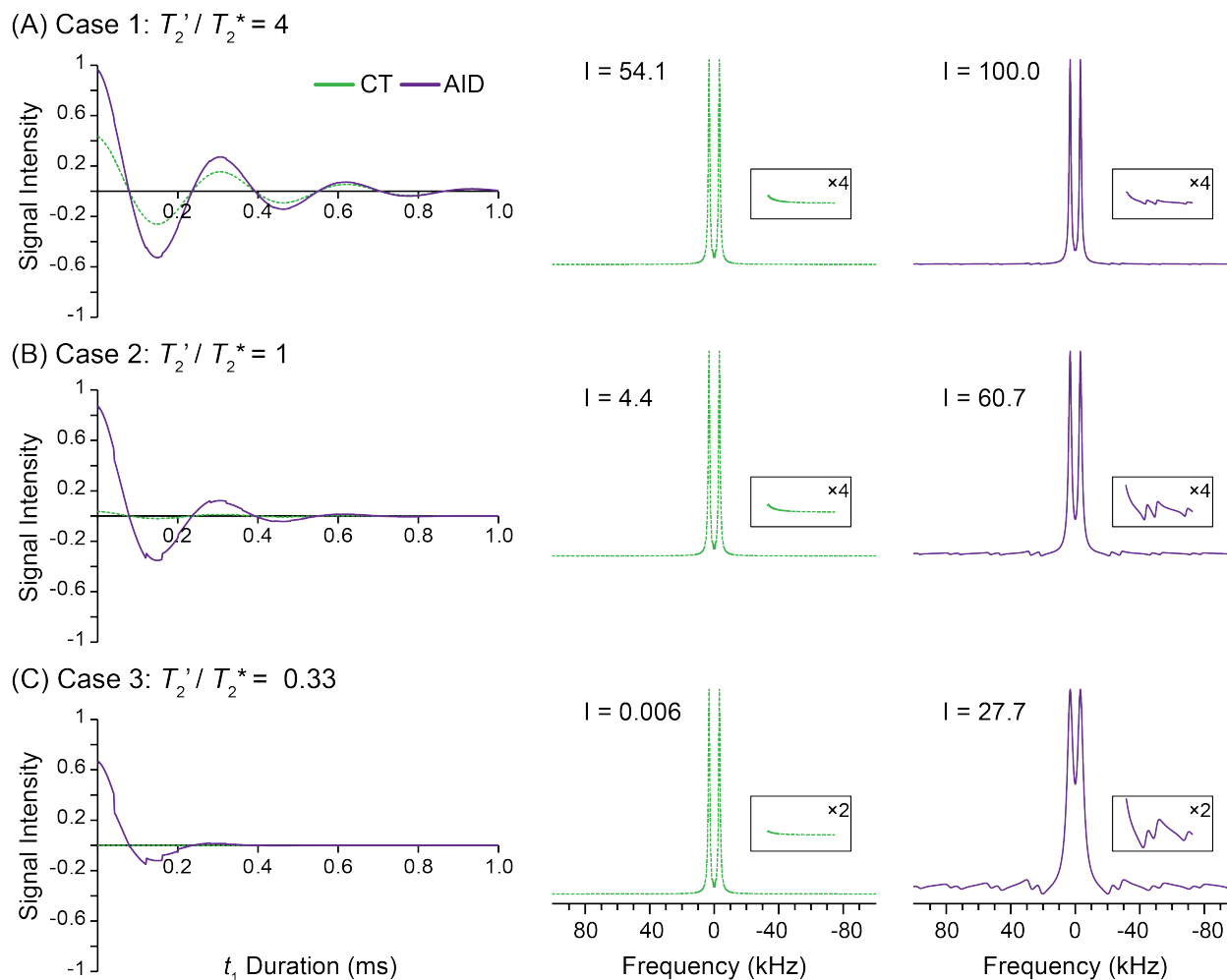


Figure 2. (A-C, left) Simulated damped cosine functions to model the t_1 -incrementation and sensitivity losses due to homogeneous ^1H transverse relaxation (T_2') for CT D-HMQC (green, dashed line) and AID D-HMQC (purple, solid line). The inhomogeneous transverse relaxation time constant (T_2^*) of the indirect detected spin was fixed at 0.3 ms. The ratio of T_2'/T_2^* was (A) 4, (B) 1 and (C) 0.33. Spectra obtained from Fourier transformation of the corresponding cosine functions are shown for (center) CT D-HMQC and (right) AID D-HMQC. The peak intensities of the frequency spectra are normalized with respect to AID D-HMQC in case 1 (purple trace on top-right).

To confirm that AID D-HMQC does not result in any spectral artifacts, we have performed simulations that model the effects of the t_1 -incrementation used in CT and AID D-HMQC experiments (Figure 2). Cosine functions taking into account homogeneous relaxation of the ^1H spins (T_2') and inhomogeneous relaxation of the indirectly detected spins (T_2^*) were used to calculate real time domain signals for CT D-HMQC and AID D-HMQC, respectively (Figure 2, left column):

$$S_{real}(t_1) = \cos(2\pi\Omega t_1) \times \exp\left(-\frac{C\tau_r}{T_2'}\right) \times \exp\left(-\frac{t_1}{T_2^*}\right) \quad (\text{Equation 1, CT D-HMQC})$$

$$S_{real}(t_1) = \cos(2\pi\Omega t_1) \times \exp\left(-\frac{D(t_1)\tau_r}{T_2'}\right) \times \exp\left(-\frac{t_1}{T_2^*}\right) \quad (\text{Equation 2, AID D-HMQC})$$

In the above equations, the frequency offset ($2\pi\Omega$) was fixed to 20000 rad s^{-1} ($\Omega = 3183 \text{ Hz}$) and T_2^* was fixed at 0.3 ms . The time domain intensities ($S_{real}(t_1)$) were then calculated by incrementing t_1 from 0 to 1 ms in steps of $2 \mu\text{s}$, corresponding to an indirect spectral width of 500 kHz . For CT D-HMQC the value of the constant C was set to 50 to give a total echo duration of 1 ms , equal to the maximum t_1 time. For AID D-HMQC, D is equal to $2, 4, 6, \dots, 50$ and is stepped to fulfill the condition $D \times \tau_r > t_1$, as described above. The $^1\text{H } T_2'$ was set to $1.2, 0.3$ and 0.1 ms in cases 1, 2 and 3, respectively, with the first and middle values being representative of typical fast MAS experiments on fully protonated solids. The imaginary FID had zero amplitude for all time points. The resulting complex FIDs were then Fourier transformed to obtain the frequency domain spectra (Figure 2, middle and right columns), which is a doublet with a splitting of 6366 Hz .

In case 1 where T_2'/T_2^* is set to 4 , there is a factor 1.8 gain in signal intensity with AID (peak intensity, $I = 100.0$ with AID and $I = 54.1$ with CT) as indicated in the Fourier transformed peaks (Figure 2A). In cases 2 and 3, as the ratio T_2'/T_2^* decreases to 1 and 0.33 , respectively, AID provides significantly higher peak intensities than the CT scheme by factors 13.8 ($60.7/4.4$) and 4616 ($27.7/0.006$), respectively (Figure 2B and 2C). Therefore, the sensitivity gain with AID increases as the $^1\text{H } T_2'$ decreases and/or when the indirect dimension acquisition time increases. However, for shorter values of $^1\text{H } T_2'$, step function artefacts become visible in the FIDs. The steps are particularly apparent in case 3 (Figure 2C, left). As a consequence, distortions which are separated by the inverse of the period of the steps ($1/40 \mu\text{s} = 25 \text{ kHz}$, in this case) appear in the

baseline of the frequency domain spectrum. The insets in the frequency spectra shown in Figure 2 compare portions of the baseline with both CT and AID schemes. The CT scheme does not introduce any baseline distortions. However, the magnitude of the baseline distortions with AID is small (ca. 3 % of the main signal in case 3) and will likely be obscured by thermal noise and t_1 -noise, both of which are absent in the simulations shown in Figure 2. Note that these distortions are similar to those obtained when using the FIREMAT experiment, which also leads to a stepped decay signal.⁵⁷

In summary, the experiments and simulations demonstrate that AID D-HMQC provides better sensitivity than CT D-HMQC. Therefore, we recommend that AID D-HMQC be used when rotor-asynchronous indirect dimension spectral widths (F_1) and Δt_1 are required. Finally, we note that if $\Delta t_1 = 2 \times \tau_r$ then AID D-HMQC and conventional, rotor-synchronized D-HMQC experiments are identical. Therefore, the pulse sequence for AID D-HMQC can also be used for rotor-synchronized experiments.

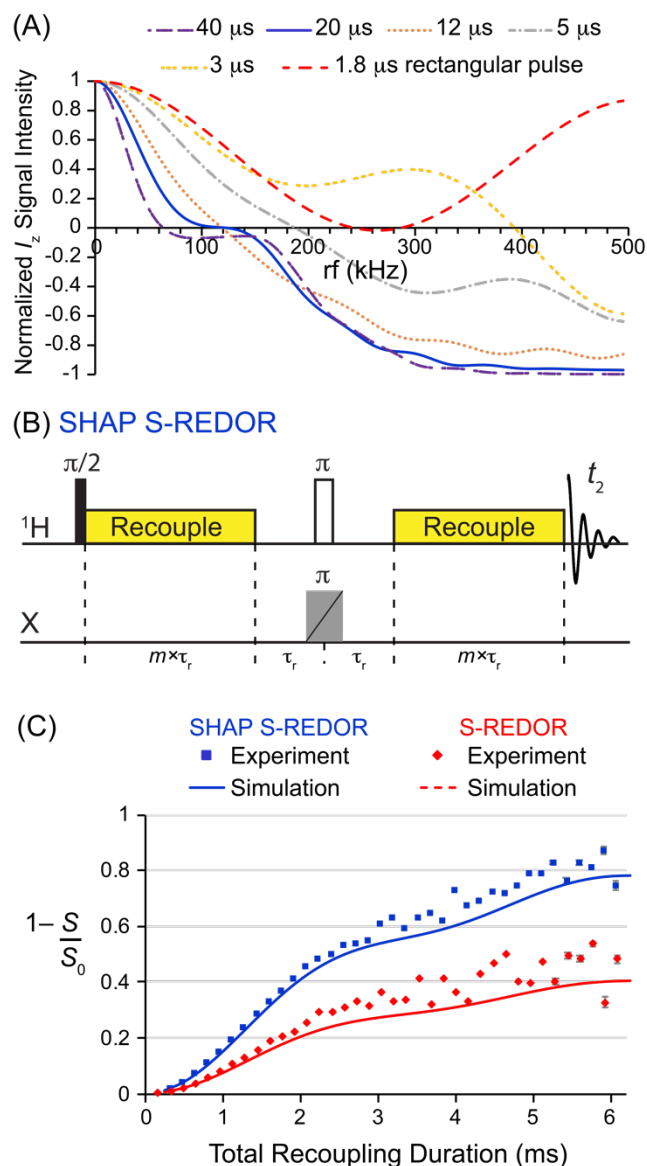


Figure 3. (A) Plot showing the SIMPSON simulated inversion efficiency as a function of rf field for tanh/tan SHAPs with different durations and sweep widths. The sweep width of the SHAPs were either 5 MHz (for 40, 20, 12 and 5 μs duration) or 3 MHz (for 3 μs duration). A 1.8 μs rectangular pulse is also included for comparison. (B) SHAP S-REDOR pulse sequence. (C) Plot showing SIMPSON simulations and experimental $^1\text{H}\{^{195}\text{Pt}\}$ SHAP S-REDOR (20 μs SHAP at 275 kHz rf) and conventional S-REDOR (1.8 μs π pulse on the X channel) curves with cisplatin. Experimental S-REDOR curves were obtained by acquiring control (S_0) and dephased (S) datasets in an interleaved fashion, and plotting the normalized difference signal $(S_0 - S)/S_0$ as a function of recoupling duration. Error bars are derived from the SNR of the S_0 and S spectra and do not account for MAS instability. Experiments were performed with a 6 s recycle delay and 16 scans. Simulations used the rep320 crystal file with (A) 17 or (C) 33 gamma angles. The MAS frequency was 50 kHz and the ^{195}Pt CSA parameters were set to model the ^{195}Pt site in cisplatin ($\Omega = 8975$ ppm, $\kappa = -0.96$) in all simulations. The SHAP pulse was applied near the 2nd positive sideband, which approximately corresponds to the median frequency of the MAS powder pattern.

SHAPs for inversion of high-CSA ^{195}Pt sites. A number of solid-state NMR experiments require efficient inversion of spins. For example, the S-REDOR pulse sequence is a recoupled heteronuclear spin echo experiment, in which simultaneous high-power rectangular π pulses are applied on the ^1H and X channels and the dephasing of the ^1H signal due to the evolution of heteronuclear dipolar couplings is observed.⁵⁸ However, rectangular pulses will offer limited efficiencies for the inversion of wide-line solid-state NMR spectra. Recently, Nishiyama and Goldbourn have demonstrated the use of phase-modulated schemes to efficiently saturate broad quadrupolar patterns in RESPDOR pulse sequences.⁵⁹ But, inversion can double the dephasing as compared to a saturation pulse for spin-1/2 nuclei. We have previously incorporated SHAPs to invert ^{195}Pt patterns in aMAT D-HMQC⁴⁰ and TONE D-HMQC schemes,⁴⁴ however, the inversion efficiency was not systematically investigated.

To test the efficiency of tanh/tan SHAPs for inversion, we have performed SIMPSON⁶⁰⁻⁶² numerical simulations. In the simulations I_z was set as the initial operator, a SHAP was applied and then I_z was set as the detect operator. Figure 3A shows the variation of the I_z with rf field for SHAPs of different duration (40, 20, 12, 5 and 3 μs) and a 1.8 μs rectangular pulse. The span (Ω) and skew (κ) of the ^{195}Pt chemical shift tensor were set to 8975 ppm and -0.96 , respectively to model the broad CSA pattern of cisplatin.³⁸ The inversion is represented by the decrease in signal intensity from 1 to -1 . From the plot, it is evident that the extent of signal inversion at a given rf field improves as the duration of the SHAP is increased from 3 to 20 μs , with no additional improvement observed above 20 μs . Using a 20 μs SHAP, the inversion efficiency is ca. 87% at an rf field of 275 kHz, which is close to the rf field strength achievable on our 1.3 mm probe with 160.0 W input power on the ^{195}Pt channel. The inversion efficiency is predicted to be about 90% at 300 kHz rf and gradually improves further when the rf is increased to 500 kHz, which is not

practically feasible with most NMR probes. These values are in good agreement with the 52% aMAT coherence transfer efficiency (as compared to a D-HMQC experiment) we were able to achieve when applying six 20 μ s 275 kHz SHAP pulses, corresponding to an inversion efficiency of $(52\%)^{1/6} = 90\%$.⁴⁰

We then tested the efficiency of SHAPs for inversion using $^1\text{H}\{^{195}\text{Pt}\}$ S-REDOR experiments and simulations on cisplatin. Figure 3B shows the SHAP S-REDOR pulse sequence in which the standard high-power rectangular π pulse is replaced by a SHAP on the X channel. The dephasing difference signal $(1-S/S_0)$ is plotted as a function of the total recoupling duration (Figure 3C). Since ^{195}Pt has a low natural abundance of 33.38%, a maximum $1-S/S_0$ value of only 0.338 is expected in the case of an isolated spin pair. In the experimental S-REDOR curves, at the same recoupling duration of 2.08 ms the SHAP leads to nearly twice the dephasing in comparison to the rectangular pulse ($1-S/S_0$ is 0.45 and 0.25 for SHAP and rectangular pulse, respectively). The dephasing is greater than the theoretical maximum due to additional dipolar couplings to the distant ^{195}Pt spins of the neighboring molecules in the lattice, which also cause the steady increase of the S-REDOR intensity at longer recoupling durations. We have previously observed this effect in a molecular Pt-based organometallic compound.⁴⁴ Furthermore, the dynamics of the NH_3 groups in cisplatin partially averages the Pt-H dipolar couplings which leads to a slower build-up of the S-REDOR curves.

To simulate these S-REDOR curves using SIMPSON, we first calculated the ^1H - ^{195}Pt dipolar couplings between ^1H and the nearest ^{195}Pt neighbors based on the previously reported crystal structure of alpha-cisplatin.⁶³ To account for the dynamics, the dominant dipolar coupling of 1510 Hz (corresponding to a 2.59 Å distance) was averaged based on the H-Pt-N bond angle of 22° , which results in a scaling of the dipolar coupling by a factor 0.79 ($0.5 \times [3\cos^2 22^\circ - 1]$).⁶⁴

Dynamical averaging was ignored when calculating the dipolar couplings to the distant ^{195}Pt spins in the lattice. Next, the probability of encountering a ^{195}Pt spin m at a given distance from a ^1H spin (denoted as p_m) based on the natural abundance of ^{195}Pt was calculated with equation 3:

$$p_m = 1 - 0.662^n \quad (3)$$

where n is the number of Pt atoms at that distance. The probability of a ^{195}Pt spin to be the nearest to cause dephasing (denoted as P_m) was then calculated with equation 4:

$$P_m = (1 - \sum_{i=1}^{m-1} P_i) \times p_m \quad (4)$$

P_1 was set to 0.338 for first ^{195}Pt spin ($m = 1$) at the nearest possible distance of 2.59 Å. The values of p_m and P_m are summarized in Table S1. Two-spin ^1H - ^{195}Pt SIMPSON simulations were performed to predict the dephasing induced by S-REDOR pulse sequences using a 20 μs SHAP with 270 kHz rf field or a 1.8 μs rectangular π -pulse with 278 kHz rf field, for each ^1H - ^{195}Pt dipolar coupling within 1 nm extracted from the crystal structure for α -cisplatin.⁶³ Finally, all the simulated curves were summed by weighting each curve by their respective probabilities (P_m). The resulting simulated S-REDOR curves show remarkable agreement with the experiments especially at short recoupling times (Figure 3C). Notably the increased dephasing obtained with SHAPs was both predicted by simulations and experimentally verified, demonstrating that the use of SHAP inversion pulses in S-REDOR permits more precise inter-nuclear distance measurements.

the TONE D-HMQC family of pulse sequences that reduce t_1 -noise by refocusing ^1H CSA across each recoupling block to improve robustness to MAS frequency fluctuations, and use flip-back or trim pulses to decrease the intensity of uncorrelated ^1H magnetization.⁴³⁻⁴⁴ TONE D-HMQC requires the application of inversion pulses to the indirectly detected spin. Here, SHAPs are incorporated into TONE D-HMQC pulse sequences to provide efficient inversion of the indirectly detected spin. The accompanying reductions in t_1 -noise and gains in sensitivity achieved with TONE D-HMQC are experimentally investigated for ^{195}Pt solid-state NMR.

Figure 4 shows pulse sequences for AID D-HMQC and TONE D-HMQC-2, -4, and -5 with the corresponding 2D $^1\text{H}\{^{195}\text{Pt}\}$ spectra of cisplatin. The $^1\text{H}\{^{195}\text{Pt}\}$ AID D-HMQC spectrum had a low ^{195}Pt sensitivity of $0.8 \text{ min}^{-1/2}$ (Figure 4B). Note that the AID D-HMQC spectrum shown in Figure 4B was obtained several months after that shown in Figure 1D and 1E. The AID D-HMQC spectrum in Figure 1D gave a higher ^{195}Pt sensitivity of $2.1 \text{ min}^{-1/2}$. When the spectra shown in Figure 4 were obtained, the MAS frequency was less stable, resulting in more t_1 -noise and reduced sensitivity (Figure S4). Figure 4C shows the modified TONE D-HMQC-2 pulse sequence which also incorporates the AID t_1 -incrementation scheme. The 2D $^1\text{H}\{^{195}\text{Pt}\}$ TONE D-HMQC-2 spectrum shows a ^{195}Pt sensitivity of $6.3 \text{ min}^{-1/2}$, providing a factor 8 gain in sensitivity in comparison to AID D-HMQC ($6.3 \text{ min}^{-1/2}/0.8 \text{ min}^{-1/2}$). TONE D-HMQC-1 shows a slightly lower ^{195}Pt sensitivity of $4.6 \text{ min}^{-1/2}$ (Figure S5); this is expected because the TONE D-HMQC-2 sequence includes a perfect echo symmetry that improves the refocusing of ^1H - ^1H homonuclear dipolar couplings and the added $\pi/2$ pulse helps to eliminate uncorrelated ^1H NMR signals.⁴³ Figure 4E shows the TONE D-HMQC-4 scheme that enhances the sensitivity of CT experiment by lengthening the ^1H T_2' . This is achieved by applying Lee-Goldburg (LG) pulses⁶⁵ to spin-lock the anti-phase/multiple quantum magnetization. Relaxation occurs during the LG spin-lock pulses

due to rotating frame relaxation and residual ^1H spin diffusion,⁶⁶ this phenomenon is highly sample dependent. In case of cisplatin, TONE D-HMQC-4 shows sensitivity of $5.9 \text{ min}^{-1/2}$ which is only slightly lower in comparison to AID TONE D-HMQC-2 (Figure 4F). In principle, the sensitivity of TONE D-HMQC-4 can be further improved by incorporating the AID scheme for t_1 -incrementation; however, this would result in a shorter LG spin-lock duration (a few rotor cycles) in the first few t_1 increments that is insufficient to suppress t_1 -noise. To overcome this problem, the AID TONE D-HMQC-5 sequence includes an additional constant duration LG spin-lock pulse to saturate uncorrelated signals and reduce t_1 -noise (Figure 4G). The corresponding 2D spectrum shown in Figure 4H showed a similar sensitivity ($5.7 \text{ min}^{-1/2}$) as TONE D-HMQC-4 suggesting that the performance of the two sequences is similar in case of cisplatin. However, AID TONE D-HMQC-5 will likely provide improved sensitivity in samples where relaxation losses under LG spin-lock pulses is an issue.

Finally, the extent of t_1 -noise was directly quantified by measuring the ratio of the noise levels in the two dimensions (t_1 -noise/thermal-noise $\approx \text{SNR}_{1\text{H}}/\text{SNR}_{195\text{Pt}}$, Table S2). AID D-HMQC showed a high amount of t_1 -noise, 6.2 higher than the thermal noise (Figure 4B), whereas, AID TONE D-HMQC-2 and -5 have equal noise levels in both dimensions, indicating complete suppression of t_1 -noise. This observation is consistent with the 8-fold higher ^{195}Pt sensitivity obtained with the TONE sequences.

In summary, we have shown that over an order of magnitude gain in sensitivity can be obtained by eliminating constant-time intervals and t_1 -noise in D-HMQC sequences for the indirect detection of ^{195}Pt spins. AID TONE D-HMQC-2 is straightforward in terms of experimental setup and is therefore suggested as the method of choice, followed by AID TONE D-HMQC-5.

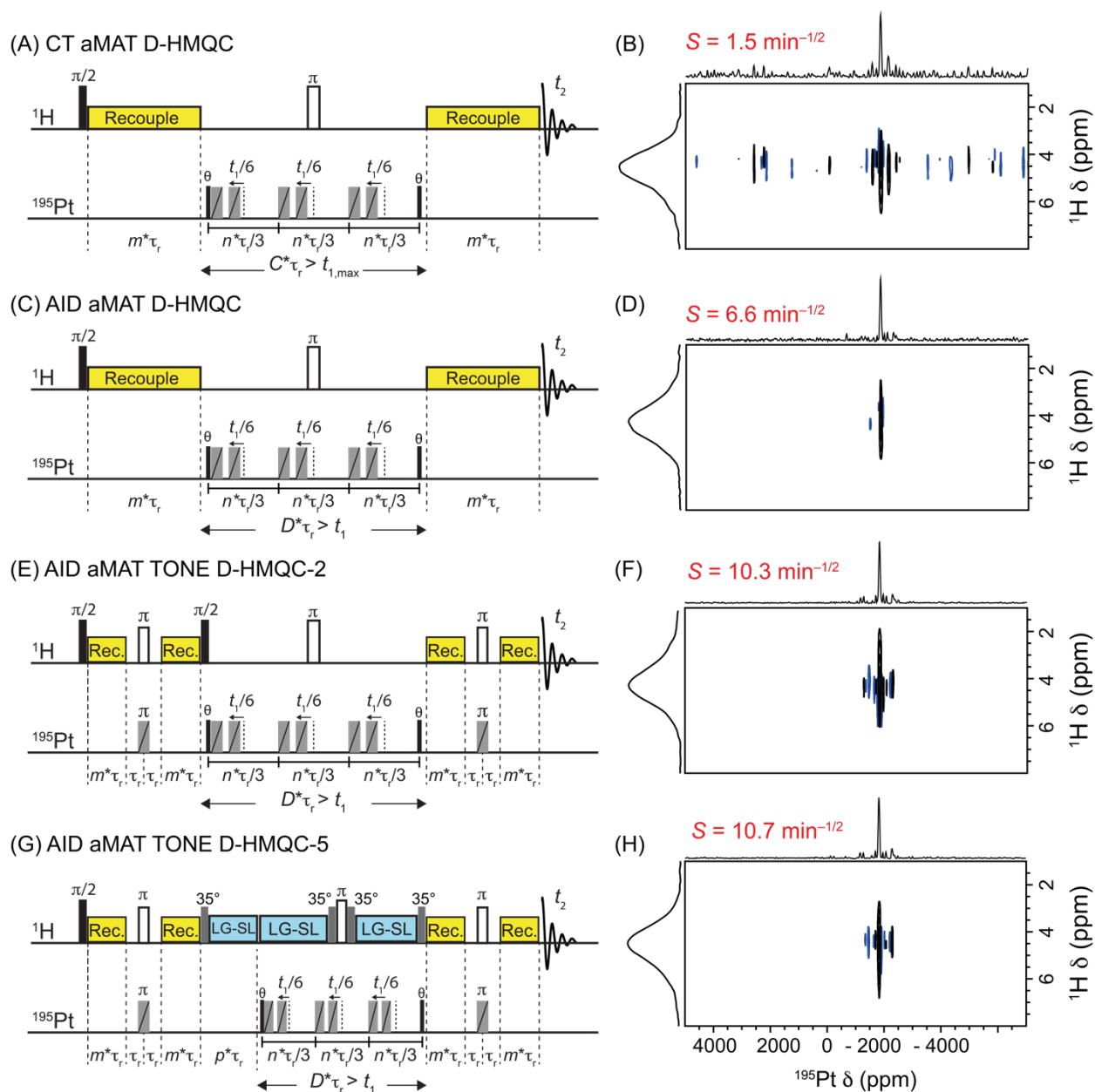


Figure 5. (A) CT aMAT D-HMQC, (C) AID aMAT D-HMQC, (E) AID aMAT TONE D-HMQC-2 and (G) AID aMAT TONE D-HMQC-5 pulse sequences and (B, D, F, H) the corresponding 2D $^1\text{H}\{^{195}\text{Pt}\}$ D-HMQC spectra of cisplatin. The sensitivity of the ^{195}Pt dimension was measured on the positive projection and is indicated above each 2D spectrum. Residual spinning sidebands (at integer multiples of $\pm 0.5\nu_r$) are observed beside the most intense isotropic signal due to the relatively long duration of the SHAP pulses (see reference [40]). Small amounts of impurities are also present ($\delta_{\text{iso}} = -2353$ ppm). Spectra were acquired with a 1 s recycle delay, (B) 42 scans or (D, F, H) 98 scans, an indirect spectral width of 1.25 MHz and 246 t_1 increments. The States scheme was used for quadrature in t_1 .

Combining TONE D-HMQC and Adiabatic MAT. The TONE scheme can also be applied to aMAT D-HMQC sequences that yield isotropic NMR spectra in the indirect dimension.⁴⁰ As

previously demonstrated, samples that have multiple ^{195}Pt sites will particularly benefit from aMAT techniques, and the refocusing of spinning sidebands into the centerband additionally improves sensitivity.⁴⁰ Figure 5A shows the $^1\text{H}\{^{195}\text{Pt}\}$ CT aMAT D-HMQC pulse sequence⁴⁰ and the corresponding 2D NMR spectrum of cisplatin. Clearly, t_1 -noise is present in the standard aMAT D-HMQC and the ^{195}Pt sensitivity is $1.5 \text{ min}^{-1/2}$ (Figure 5B). Analogous to what was noted above, the AID scheme provides a significant boost in sensitivity and shows a ^{195}Pt sensitivity of $6.6 \text{ min}^{-1/2}$ (Figure 5C and 5D). Simulations predict that the introduction of the AID scheme into aMAT D-HMQC creates artefacts with lower intensity than the residual spinning sidebands (Figure S6 and S7). The application of aMAT TONE D-HMQC-2 and -5 sequences further improves the sensitivity to 10.3 and $10.7 \text{ min}^{-1/2}$, respectively by reducing t_1 -noise. As a result, the overall sensitivity is improved by a factor 7 ($10.7 \text{ min}^{-1/2} / 1.5 \text{ min}^{-1/2}$) using aMAT TONE D-HMQC-5, in comparison to the standard CT aMAT D-HMQC. Notably, we were able to utilize this improved sensitivity to acquire a 2D $^1\text{H}\{^{195}\text{Pt}\}$ aMAT D-HMQC spectrum in only 6 minutes and observe the ^{195}Pt isotropic signal of cisplatin (Figure S8).

Alternatively, the various TONE schemes may also be implemented into the CT aMAT D-HMQC sequence (Figure S9). The CT aMAT TONE D-HMQC-2 sequence shows a ^{195}Pt sensitivity of $7.7 \text{ min}^{-1/2}$ (Figure S9F) whereas the CT aMAT TONE D-HMQC-4 shows a marked sensitivity improvement to $9.1 \text{ min}^{-1/2}$, likely due to lengthening of ^1H coherence lifetimes under the LG pulses during the constant ^1H echo period. The relative performance of the AID and CT aMAT TONE D-HMQC schemes is sample-dependent but the AID schemes will likely provide similar or greater sensitivities. We note that the isotropic shifts can also be readily obtained by acquiring rotor-synchronized 2D TONE D-HMQC-2 spectra at two different MAS frequencies,^{41-42, 44} but this approach may be challenging with samples containing several sites, or 767 sites with

distributions of isotropic chemical shifts. For instance, our previously-studied Pt/UiO-66-NH₂ metal-organic framework featured two sites with isotropic ¹⁹⁵Pt linewidths at half-height of 25 kHz at 9.4 T.⁴⁰ In summary, AID TONE D-HMQC-2 provides the highest sensitivity to indirectly detect ¹⁹⁵Pt spinning sideband manifolds, whereas AID aMAT TONE D-HMQC-5 provides the best sensitivity to obtain purely isotropic ¹⁹⁵Pt NMR spectra. We would also like to note that the described modifications to aMAT D-HMQC can also be performed with MAT D-HMQC,⁴⁰ as the relative sensitivity of the aMAT or MAT D-HMQC methods will likely vary with the quality factor of the probe.

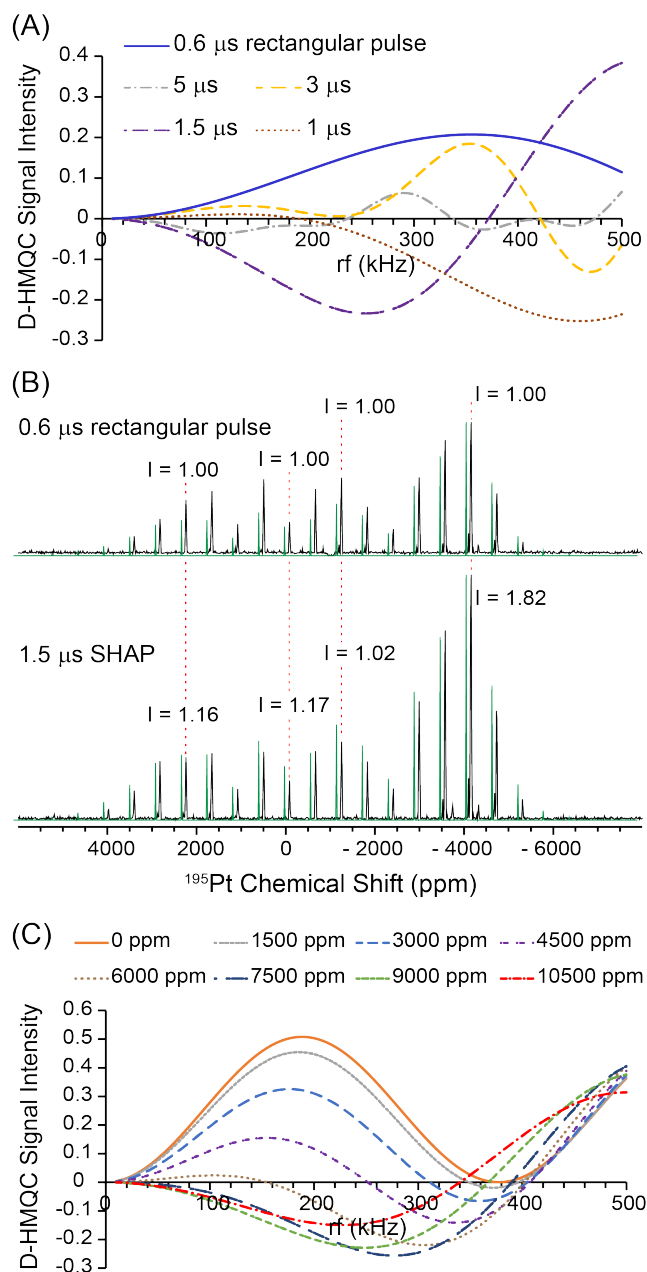


Figure 6. (A) Plot showing the SIMPSON simulated variation of $^1\text{H}\{^{195}\text{Pt}\}$ D-HMQC signal intensity with rf field for different ^{195}Pt excitation pulses (0.6 μs rectangular pulse, and 5, 3, 1.5 and 1 μs tanh/tan pulses). The sweep widths of the tanh/tan pulses were either 5 MHz (for 5 μs pulse) or 3 MHz (for 3, 1.5 and 1 μs pulses). Simulations used ^{195}Pt $\Omega = 8975$ ppm and $\kappa = -0.96$ to model cisplatin. (B) Comparison of (black traces) ^{195}Pt positive projections from 2D $^1\text{H}\{^{195}\text{Pt}\}$ AID TONE D-HMQC-2 spectra acquired with a (top) 0.6 μs rectangular pulse and a (bottom) 1.5 μs tanh/tan pulse. The relative signal intensities of a few sidebands are indicated. Analytical simulations with $\delta_{\text{iso}} = -1834$ ppm, $\Omega = 8975$ ppm and $\kappa = -0.96$ are shown in green. (C) Plot showing the SIMPSON simulated variation of D-HMQC signal intensity with 1.5 μs tanh/tan excitation and different rf fields for the indicated ^{195}Pt Ω values ($\kappa = -1$ in all cases). Simulations used the rep168 crystal file with 17 gamma angles.

Swept-Excitation Pulses. Finally, we explore the possibility of using swept pulses for the broadband excitation of ^{195}Pt signals in D-HMQC experiments instead of the standard short-duration, high-power rectangular pulses. Swept pulses at low rf powers may enable more widespread application of D-HMQC sequences given that rectangular excitation pulses require high rf fields (ca. 275 kHz was used here).³⁸ Figure 6A shows SIMPSON simulations of the $^1\text{H}\{^{195}\text{Pt}\}$ D-HMQC signal intensity using a 0.6 μs rectangular pulse (similar to D-HMQC experiments shown above) and tanh/tan pulses of durations 5, 3, 1.5 and 1 μs , as a function of the rf field. Simulations were performed with a ^{195}Pt span (Ω) and skew (κ) of 8975 ppm and -0.96 , respectively, to model cisplatin. The 0.6 μs rectangular pulse, previously shown to provide an optimal excitation, displays a simulated maximum D-HMQC signal of 0.21 at 360 kHz rf (*i.e.*, the simulations indicate an efficiency of 21% for D-HMQC with a ^1H - ^{195}Pt spin pair), however, at a more practical rf field of 280 kHz, the HMQC signal is reduced to 0.18 (Figure 6A). The excitation efficiency of tanh/tan pulses is improved upon reduction of the pulse duration to ≤ 3 μs . Below an rf field strength of 300 kHz, only the 1.5 μs tanh/tan pulse is found to provide a good HMQC efficiency with the simulated maximum signal at 250 kHz rf being -0.23 . A comparison of the predicted absolute D-HMQC signal with the 1.5 μs tanh/tan pulse and 0.6 μs rectangular pulse shows an overall gain in efficiency by a factor 1.3 (0.23/0.18), suggesting that tanh/tan pulses may provide signal enhancements over standard rectangular pulses for excitation.

Figure 6B shows the ^{195}Pt projection from 2D $^1\text{H}\{^{195}\text{Pt}\}$ AID TONE D-HMQC-2 experiments obtained with a 0.6 μs rectangular pulse (Figure 4D) and 1.5 μs tanh/tan pulse. Notably, the 1D $^1\text{H}\{^{195}\text{Pt}\}$ signals (first slice of 2D spectra) were opposite in phase as predicted by the simulations (Figure 6A). In the ^{195}Pt spectrum obtained with the tanh/tan pulse, the sideband signal intensities are markedly higher across the ^{195}Pt pattern, with gains in sideband intensities by

factors between 1.02 and 1.82. The benefit of using swept pulses for excitation is clear when the experimental sideband manifold is compared with analytical simulations. As shown in Figure 6B, the analytical simulation (green trace) based on expected ^{195}Pt CSA tensor parameters, fits more closely to the experimental spectrum obtained with the $1.5\ \mu\text{s}$ tanh/tan pulse in comparison to the $0.6\ \mu\text{s}$ rectangular pulse. Particularly, the relative intensities of the sidebands near 2000 and -4000 ppm are more accurately reproduced. These results clearly suggest that swept pulses may provide signal enhancements in addition to providing a more accurate ^{195}Pt sideband manifold that rivals direct detection experiments.

One caveat with the use of full sweeps for excitation is the strong dependence of the excitation efficiency on the ^{195}Pt CSA. Figure 6C compares SIMPSON simulations of the $^1\text{H}\{^{195}\text{Pt}\}$ D-HMQC signal using a $1.5\ \mu\text{s}$ tanh/tan and different ^{195}Pt Ω values. In all cases, the ^{195}Pt transmitter was placed approximately at the center of the sideband manifold for uniform excitation, similar to the experiments. For all Ω values, the D-HMQC efficiency is high above 450 kHz rf. However, within a more practically accessible rf field range of 0 to 300 kHz, the D-HMQC signal intensity reduces dramatically upon increasing Ω from 0 to 6000 ppm. A relatively high D-HMQC signal intensity (> 0.3) is retained until $\Omega = 3000$ ppm at rf fields near 180-200 kHz, whereas when $\Omega = 7500$ ppm the highest efficiency is obtained with an rf field of ca. 280 kHz. As cisplatin has a ^{195}Pt $\Omega = 8975$ ppm, a reasonable excitation efficiency of -0.23 was retained at ca. 250 kHz rf. Figure S10 compares the dependence of different excitation pulses with CSA. These simulations suggest that optimal excitation conditions for different CSA can likely be fine-tuned by varying the pulse duration between 1 and 3 μs , however, such an endeavor is outside the scope of this work.

In summary, swept excitation pulses may provide improved excitation and more accurate reproduction of ^{195}Pt sideband manifolds in comparison D-HMQC experiments with rectangular pulses. But, optimal SHAP conditions (pulse duration, rf field and sweep width) vary depending on the CSA of the indirectly detected spin. This problem can easily be addressed by quickly experimentally testing various excitation pulse conditions with 1D D-HMQC experiments to identify which work best for a given sample. The best performing excitation pulse can then be used for the more time consuming 2D experiments.

Conclusions

We have shown that the sensitivity of indirect detection experiments with heavy spin-1/2 nuclei such as ^{195}Pt can be enhanced with improved D-HMQC and S-REDOR pulse sequences. Arbitrary Indirect Dwell (AID) D-HMQC showed a factor 1.3 to 2.6 improvement in ^{195}Pt sensitivity in comparison to constant-time (CT) D-HMQC, with the gain in sensitivity dependent upon the maximum t_1 -evolution time. AID D-HMQC can be applied for the indirect detection of solid-state NMR spectra in general, as demonstrated with experiments on the half-integer quadrupolar nucleus ^{35}Cl . Simulations demonstrate that AID t_1 -incrementation introduces negligible distortions in the indirect dimension spectrum. Numerical simulations and experiments showed that SHAPs can successfully invert wideline MAS ^{195}Pt patterns, even in the presence of extreme CSA > 8000 ppm. The SHAP can then be incorporated into S-REDOR experiments to enhance dipolar dephasing and used in TONE D-HMQC sequences to reduce t_1 -noise. Notably, a $20\ \mu\text{s}$ SHAP with 5 MHz sweep width provided a factor two higher dephasing in comparison to a high-power rectangular pulse in S-REDOR experiments. The higher dephasing will result in more precise ^1H - ^{195}Pt distance measurements under fast MAS conditions. SHAPs were also incorporated

in TONE D-HMQC schemes that necessitate an inversion pulse on the X channel. Notably, the $^1\text{H}\{^{195}\text{Pt}\}$ AID TONE D-HMQC experiment showed an order of magnitude improvement in sensitivity in comparison to AID D-HMQC due to the elimination of t_1 -noise. The incorporation of AID and TONE into aMAT D-HMQC experiments showed a factor 7.1 improvement in sensitivity over standard aMAT D-HMQC due to t_1 -noise suppression and longer ^1H coherence times during the constant-time echo duration. Finally, we showed that swept pulses can also potentially replace rectangular pulses for excitation in indirect detection D-HMQC experiments. The use of a $1.5\ \mu\text{s}$ tanh/tan resulted in a more accurate ^{195}Pt sideband manifold of cisplatin and gains in sideband signal intensities on the order 1.02-1.82.

Using the methods proposed here, it should be possible to characterize Pt sites present in low-concentration on the surfaces of materials or in porous materials such as zeolites, metal organic frameworks and covalent organic frameworks, applicable in heterogeneous catalysis. The improved schemes demonstrated here with ^{195}Pt should also find application to other moderately-abundant, heavy spin-1/2 nuclei such as ^{113}Cd , ^{119}Sn , ^{125}Te , ^{207}Pb , etc. that often have large CSA. These types of experiments will also become valuable with the increasing prevalence of high-field NMR systems that will exacerbate broadening of SSNMR spectra by CSA.

Experimental

cis-Diamminedichloroplatinum (II) (cisplatin) and L-histidine·HCl·H₂O were purchased and used as received from Alfa Aesar and Fluka, respectively. All solid-state NMR experiments were performed at a static magnetic field of 9.4 T with a Bruker Avance III HD console, Bruker 1.3 mm HX probe and a 50 kHz MAS frequency. Spectra were processed using the Bruker TopSpin program. The ^1H shift of adamantane (1.82 ppm) as a secondary standard to indirectly reference

the ^1H , ^{195}Pt and ^{35}Cl chemical shifts to neat tetramethylsilane, using the previously established relative Larmor frequencies.⁶⁷ In all cases, the sensitivity of the ^{195}Pt traces were calculated based on the signal-to-noise ratio of the most intense sideband at -4153 ppm. Four SNR measurements were performed by choosing different baseline regions and averaged to decrease error in the calculated sensitivities. All 2D spectra comparisons are made by plotting the contours at the same floor level.

The $\pi/2$ and π pulse durations for ^1H were 2.5 and 5 μs , and the central transition selective pulse durations for ^{35}Cl were 4.3 and 8.6 μs , respectively. The population transfer scheme⁶⁸ was implemented in the $^1\text{H}\{^{35}\text{Cl}\}$ TONE D-HMQC-3 experiments as described previously (Figure S2 and S3).⁴³ 38 μs WURST pulses with a delay of 2 μs between pulses were applied at an offset of 450 kHz and an optimized 33.5 kHz rf field. All ^{195}Pt SHAPs used tanh/tan pulse shapes that were generated on TopSpin. The ^{195}Pt pulse durations and rf fields are indicated in each section of the manuscript. All experiments used $SR4_1^2$ dipolar recoupling⁶⁹ which was applied at the 2nd order R^3 condition.⁷⁰ For the $^1\text{H}\{^{195}\text{Pt}\}$ D-HMQC experiments, the optimal total recoupling duration was either 2.16 ms (for data shown in Figure 1 and Figure S1) or 1.92 ms (for data shown in Figures 4, 5 and 6). An optimal total recoupling duration of 2.08 ms was used in the $^1\text{H}\{^{35}\text{Cl}\}$ TONE D-HMQC-3 experiments. Other relevant experimental details are provided in the figure captions.

A short quadrature spike present at the transmitter frequency in the indirect dimension of the 2D $^1\text{H}\{^{195}\text{Pt}\}$ TONE D-HMQC spectra acquired with rectangular ^{195}Pt excitation pulses (data shown in Figures 4, 5 and 6), was removed by using a qfil baseline correction mode and the setting the filter width to 0.02 ppm. To minimize the quadrature artifacts, $^1\text{H}\{^{195}\text{Pt}\}$ TONE D-HMQC experiments were performed using a COG5(1,2,1,2;0) cogwheel phase cycle⁷¹ on the ^1H channel, resulting in a short 10-step phase cycle. The standard aMAT D-HMQC pulse sequence (Figure

5A) used a COG3(2,1;0) on the ^1H channel and COG14(0,13,0,13,0,13,0,13;7) on the X channel, as described previously.⁴⁰ aMAT TONE D-HMQC pulse sequences used COG7(6,1,6,1;0) and COG14(0,13,0,13,0,13,0,13;7) on the ^1H and X channels, respectively, resulting in a 98-step phase cycle. Cogwheel phase cycles were calculated using CCCP++.⁷²

Simulations modeling CT and AID D-HMQC shown in Figure 2 were performed by processing the time-domain signals in ssNAKE v1.1.⁷³ The time-domain cosine functions were zero-filled up to 2048 points before Fourier transformation. ^{195}Pt analytical simulations (shown in Figure 6) were performed in TopSpin's solid lineshape analysis (sola) module.

Acknowledgements

This work was supported by the U.S. Department of Energy (DOE), Office of Science, Basic Energy Sciences, Materials Science and Engineering Division. The Ames Laboratory is operated for the U.S. DOE by Iowa State University under contract # DE-AC02-07CH11358.

Supporting Information

Additional supplementary figures, pulse programs and shape files, and a video illustrating CT and AID D-HMQC can be found in the supporting information.

References

1. Fitzgerald, J. J.; DePaul, S. M. Solid-State NMR Spectroscopy of Inorganic Materials: An Overview. In *Solid-State NMR Spectroscopy of Inorganic Materials*, American Chemical Society: 1999; Vol. 717, pp 2-133.
2. Chmelka, B. F. Materializing opportunities for NMR of solids. *J. Magn. Reson.* **2019**, *306*, 91-97.
3. Chien, P.-H.; Griffith, K. J.; Liu, H.; Gan, Z.; Hu, Y.-Y. Recent Advances in Solid-State Nuclear Magnetic Resonance Techniques for Materials Research. *Annual Review of Materials Research* **2020**, *50* (1), 493-520.
4. Lucier, B. E. G.; Johnston, K. E.; Xu, W. Q.; Hanson, J. C.; Senanayake, S. D.; Yao, S. Y.; Bourassa, M. W.; Srebro, M.; Autschbach, J.; Schurko, R. W. Unravelling the Structure of Magnus' Pink Salt. *J. Am. Chem. Soc.* **2014**, *136* (4), 1333-1351.
5. Lucier, B. E. G.; Reidel, A. R.; Schurko, R. W. Multinuclear Solid-State NMR of Square-Planar Platinum Complexes - Cisplatin and Related Systems. *Canadian Journal of Chemistry-Revue Canadienne De Chimie* **2011**, *89* (7), 919-937.
6. Sparks, S. W.; Ellis, P. D. ^{195}Pt Shielding Tensors in Potassium Hexachloroplatinate(IV) and Potassium Tetrachloroplatinate(II). *J. Am. Chem. Soc.* **1986**, *108* (12), 3215-3218.

7. Massiot, D.; Farnan, I.; Gautier, N.; Trumeau, D.; Trokner, A.; Coutures, J. P. ⁷¹Ga and ⁶⁹Ga Nuclear-Magnetic-Resonance Study of Beta-Ga₂O₃ - Resolution of 4-Fold and 6-Fold Coordinated Ga Sites in Static Conditions. *Solid State Nucl. Magn. Reson.* **1995**, *4* (4), 241-248.
8. Yamauchi, K.; Janssen, J. W. G.; Kentgens, A. P. M. Implementing solenoid microcoils for wide-line solid-state NMR. *J. Magn. Reson.* **2004**, *167* (1), 87-96.
9. Schurko, R. W. Ultra-Wideline Solid-State NMR Spectroscopy. *Acc. Chem. Res.* **2013**, *46* (9), 1985-1995.
10. Kupce, E.; Freeman, R. Adiabatic Pulses for Wide-Band Inversion and Broad-Band Decoupling. *J. Magn. Reson., Ser. A* **1995**, *115* (2), 273-276.
11. Bhattacharyya, R.; Frydman, L. Quadrupolar nuclear magnetic resonance spectroscopy in solids using frequency-swept echoing pulses. *J. Chem. Phys.* **2007**, *127* (19).
12. Larsen, F. H.; Jakobsen, H. J.; Ellis, P. D.; Nielsen, N. C. Sensitivity-enhanced quadrupolar-echo NMR of half-integer quadrupolar nuclei. Magnitudes and relative orientation of chemical shielding and quadrupolar coupling tensors. *J. Phys. Chem. A* **1997**, *101* (46), 8597-8606.
13. MacGregor, A. W.; O'Dell, L. A.; Schurko, R. W. New Methods for the Acquisition of Ultra-Wideline Solid-State NMR Spectra of Spin-1/2 Nuclides. *J. Magn. Reson.* **2011**, *208* (1), 103-113.
14. Harris, K. J.; Lupulescu, A.; Lucier, B. E. G.; Frydman, L.; Schurko, R. W. Broadband Adiabatic Inversion Pulses for Cross Polarization in Wideline Solid-State NMR Spectroscopy. *J. Magn. Reson.* **2012**, *224*, 38-47.
15. Altenhof, A. R.; Jaroszewicz, M. J.; Harris, K. J.; Schurko, R. W. Broadband adiabatic inversion experiments for the measurement of longitudinal relaxation time constants. *The Journal of Chemical Physics* **2021**, *154* (3), 034202.
16. Kobayashi, T.; Perras, F. A.; Goh, T. W.; Metz, T. L.; Huang, W. Y.; Pruski, M. DNP-Enhanced Ultrawideline Solid-State NMR Spectroscopy: Studies of Platinum in Metal-Organic Frameworks. *J. Phys. Chem. Lett.* **2016**, *7* (13), 2322-2327.
17. Kobayashi, T.; Perras, F. A.; Murphy, A.; Yao, Y.; Catalano, J.; Centeno, S. A.; Dybowski, C.; Zumbulyadis, N.; Pruski, M. DNP-enhanced ultrawideline Pb-207 solid-state NMR spectroscopy: an application to cultural heritage science. *Dalton Trans.* **2017**, *46* (11), 3535-3540.
18. Camacho-Bunquin, J.; Ferrandon, M.; Sohn, H.; Yang, D. L.; Liu, C.; Ignacio-de Leon, P. A.; Perras, F. A.; Pruski, M.; Stair, P. C.; Delferro, M. Chemoselective Hydrogenation with Supported Organoplatinum(IV) Catalyst on Zn(II)-Modified Silica. *J. Am. Chem. Soc.* **2018**, *140* (11), 3940-3951.
19. Hung, I.; Zhou, L. N.; Pourpoint, F.; Grey, C. P.; Gan, Z. H. Isotropic High Field NMR Spectra of Li-Ion Battery Materials with Anisotropy > 1 MHz. *J. Am. Chem. Soc.* **2012**, *134* (4), 1898-1901.
20. Hu, Y. Y.; Levin, E. M.; Schmidt-Rohr, K. Broadband "Infinite-Speed" Magic-Angle Spinning NMR Spectroscopy. *J. Am. Chem. Soc.* **2009**, *131* (24), 8390-+.
21. Piveteau, L.; Ong, T. C.; Walder, B. J.; Dirin, D. N.; Moscheni, D.; Schneider, B.; Bar, J.; Protesescu, L.; Masciocchi, N.; Guagliardi, A.; Emsley, L.; Coperet, C.; Kovalenko, M. V. Resolving the Core and the Surface of CdSe Quantum Dots and Nanoplatelets Using Dynamic Nuclear Polarization Enhanced PASS-PIETA NMR Spectroscopy. *Acs Central Sci* **2018**, *4* (9), 1113-1125.
22. Altenhof, A. R.; Jaroszewicz, M. J.; Lindquist, A. W.; Foster, L. D. D.; Veinberg, S. L.; Schurko, R. W. Practical Aspects of Recording Ultra-Wideline NMR Patterns under Magic-Angle Spinning Conditions. *J. Phys. Chem. C* **2020**, *124* (27), 14730-14744.
23. Demers, J. P.; Chevelkov, V.; Lange, A. Progress in correlation spectroscopy at ultra-fast magic-angle spinning: Basic building blocks and complex experiments for the study of protein structure and dynamics. *Solid State Nucl. Magn. Reson.* **2011**, *40* (3), 101-113.
24. Nishiyama, Y. Fast magic-angle sample spinning solid-state NMR at 60–100 kHz for natural abundance samples. *Solid State Nucl. Magn. Reson.* **2016**, *78*, 24-36.
25. Samoson, A.; Tuhern, T.; Past, J.; Reinhold, A.; Heinmaa, I.; Anupöld, T.; Smith, M. E.; Pike, K. J. Fast Magic-Angle Spinning: Implications. *eMagRes* **2010**.

26. Poppler, A. C.; Demers, J. P.; Malon, M.; Singh, A. P.; Roesky, H. W.; Nishiyama, Y.; Lange, A. Ultrafast Magic-Angle Spinning: Benefits for the Acquisition of Ultrawide-Line NMR Spectra of Heavy Spin-1/2 Nuclei. *ChemPhysChem* **2016**, *17* (6), 812-816.
27. Ishii, Y.; Tycko, R. Sensitivity Enhancement in Solid State ^{15}N NMR by Indirect Detection with High-Speed Magic Angle Spinning. *J. Magn. Reson.* **2000**, *142* (1), 199-204.
28. Paulson, E. K.; Morcombe, C. R.; Gaponenko, V.; Dancheck, B.; Byrd, R. A.; Zilm, K. W. Sensitive High Resolution Inverse Detection NMR Spectroscopy of Proteins in the Solid State. *J. Am. Chem. Soc.* **2003**, *125* (51), 15831-15836.
29. Wiench, J. W.; Bronnimann, C. E.; Lin, V. S. Y.; Pruski, M. Chemical Shift Correlation NMR Spectroscopy with Indirect Detection in Fast Rotating Solids: Studies of Organically Functionalized Mesoporous Silicas. *J. Am. Chem. Soc.* **2007**, *129* (40), 12076-12077.
30. Reif, B.; Griffin, R. G. ^1H Detected ^1H - ^{15}N Correlation Spectroscopy in Rotating Solids. *J. Magn. Reson.* **2003**, *160* (1), 78-83.
31. Schnell, I.; Langer, B.; Sontjens, S. H. M.; van Genderen, M. H. P.; Sijbesma, R. P.; Spiess, H. W. Inverse Detection and Heteronuclear Editing in ^1H - ^{15}N Correlation and ^1H - ^1H Double-Quantum NMR Spectroscopy in the Solid State under Fast MAS. *J. Magn. Reson.* **2001**, *150* (1), 57-70.
32. Andreas, L. B.; Jaudzems, K.; Stanek, J.; Lalli, D.; Bertarello, A.; Le Marchand, T.; Paepe, D. C. D.; Kotelovica, S.; Akopjana, I.; Knott, B.; Wegner, S.; Engelke, F.; Lesage, A.; Emsley, L.; Tars, K.; Herrmann, T.; Pintacuda, G. Structure of fully protonated proteins by proton-detected magic-angle spinning NMR. *Proc. Natl. Acad. Sci. U. S. A.* **2016**, *113* (33), 9187-9192.
33. Gan, Z. H.; Amoureux, J. P.; Trebosc, J. Proton-detected ^{14}N MAS NMR using homonuclear decoupled rotary resonance. *Chem. Phys. Lett.* **2007**, *435* (1-3), 163-169.
34. Lafon, O.; Wang, Q.; Hu, B. W.; Vasconcelos, F.; Trebosc, J.; Cristol, S.; Deng, F.; Amoureux, J. P. Indirect Detection via Spin-1/2 Nuclei in Solid State NMR Spectroscopy: Application to the Observation of Proximities between Protons and Quadrupolar Nuclei. *J. Phys. Chem. A* **2009**, *113* (46), 12864-12878.
35. Cavadini, S.; Antonijevec, S.; Lupulescu, A.; Bodenhausen, G. Indirect Detection of Nitrogen-14 in Solid-State NMR Spectroscopy. *ChemPhysChem* **2007**, *8* (9), 1363-1374.
36. Duong, N. T.; Nishiyama, Y. Satellite and central transitions selective $^1\text{H}/\{^{27}\text{Al}\}$ D-HMQC experiments at very fast MAS for quadrupolar couplings determination. *Solid State Nucl. Magn. Reson.* **2017**, *84*, 83-88.
37. Wijesekara, A. V.; Venkatesh, A.; Lampkin, B. J.; VanVeller, B.; Lubach, J. W.; Nagapudi, K.; Hung, I.; Gor'kov, P. L.; Gan, Z.; Rossini, A. J. Fast Acquisition of Proton-Detected HETCOR Solid-State NMR Spectra of Quadrupolar Nuclei and Rapid Measurement of NH Bond Lengths by Frequency Selective HMQC and RESPDOR Pulse Sequences. *Chem. Eur. J.* **2020**, *26* (35), 7881-7888.
38. Rossini, A. J.; Hanrahan, M. P.; Thuo, M. Rapid Acquisition of Wideline MAS Solid-State NMR Spectra with Fast MAS, Proton Detection, and Dipolar HMQC Pulse Sequences. *Phys. Chem. Chem. Phys.* **2016**, *18* (36), 25284-25295.
39. Clement, R. J.; Pell, A. J.; Middlemiss, D. S.; Strobridge, F. C.; Miller, J. K.; Whittingham, M. S.; Emsley, L.; Grey, C. P.; Pintacuda, G. Spin-Transfer Pathways in Paramagnetic Lithium Transition-Metal Phosphates from Combined Broadband Isotropic Solid-State MAS NMR Spectroscopy and DFT Calculations. *J. Am. Chem. Soc.* **2012**, *134* (41), 17178-17185.
40. Perras, F. A.; Venkatesh, A.; Hanrahan, M. P.; Goh, T. W.; Huang, W.; Rossini, A. J.; Pruski, M. Indirect Detection of Infinite-Speed MAS Solid-State NMR Spectra. *J. Magn. Reson.* **2017**, *276*, 95-102.
41. Li, Y. X.; Trebosc, J.; Hu, B. W.; Shen, M.; Amoureux, J. P.; Lafon, O. Indirect detection of Broad Spectra in Solid-State NMR Using Interleaved DANTE Trains. *J. Magn. Reson.* **2018**, *294*, 101-114.
42. Paluch, P.; Rankin, A. G. M.; Trebosc, J.; Lafon, O.; Amoureux, J. P. Analysis of HMQC Experiments Applied to a Spin 1/2 Nucleus Subject to Very Large CSA. *Solid State Nucl. Magn. Reson.* **2019**, *100*, 11-25.

43. Venkatesh, A.; Luan, X.; Perras, F. A.; Hung, I.; Huang, W.; Rossini, A. J. t_1 -Noise Eliminated Dipolar Heteronuclear Multiple-Quantum Coherence Solid-State NMR Spectroscopy. *Phys. Chem. Chem. Phys.* **2020**, *22*, 20815-20828.
44. Venkatesh, A.; Lund, A.; Rochlitz, L.; Jabbour, R.; Gordon, C. P.; Menzildjian, G.; Viger-Gravel, J.; Berruyer, P.; Gajan, D.; Copéret, C.; Lesage, A.; Rossini, A. J. The Structure of Molecular and Surface Platinum Sites Determined by DNP-SENS and Fast MAS ^{195}Pt Solid-State NMR Spectroscopy. *J. Am. Chem. Soc.* **2020**, *142* (44), 18936-18945.
45. Kervern, G.; Pintacuda, G.; Emsley, L. Fast Adiabatic Pulses for Solid-State NMR of Paramagnetic Systems. *Chem. Phys. Lett.* **2007**, *435* (1-3), 157-162.
46. Carvalho, J. P.; Pell, A. J. Frequency-swept adiabatic pulses for broadband solid-state MAS NMR. *J. Magn. Reson.* **2021**, *324*, 106911.
47. Hu, B.; Trebosc, J.; Amoureux, J. P. Comparison of several hetero-nuclear dipolar recoupling NMR methods to be used in MAS HMQC/HSQC. *J. Magn. Reson.* **2008**, *192* (1), 112-122.
48. Trebosc, J.; Hu, B.; Amoureux, J. P.; Gan, Z. Through-Space R^3 -HETCOR Experiments between Spin-1/2 and Half-Integer Quadrupolar Nuclei in Solid-State NMR. *J. Magn. Reson.* **2007**, *186* (2), 220-227.
49. Venkatesh, A.; Hanrahan, M. P.; Rossini, A. J. Proton Detection of MAS Solid-State NMR Spectra of Half-Integer Quadrupolar Nuclei. *Solid State Nucl. Magn. Reson.* **2017**, *84*, 171-181.
50. Lu, X.; Lafon, O.; Trebosc, J.; Tricot, G.; Delevoye, L.; Mear, F.; Montagne, L.; Amoureux, J. P. Observation of proximities between spin-1/2 and quadrupolar nuclei: Which heteronuclear dipolar recoupling method is preferable? *J. Chem. Phys.* **2012**, *137* (14), 144201.
51. Asami, S.; Reif, B. Accessing Methyl Groups in Proteins via ^1H -detected MAS Solid-state NMR Spectroscopy Employing Random Protonation. *Sci. Rep.* **2019**, *9*, 15903.
52. Straus, S. K.; Bremi, T.; Ernst, R. R. Resolution Enhancement by Homonuclear J Decoupling in Solid-State MAS NMR. *Chem. Phys. Lett.* **1996**, *262* (6), 709-715.
53. Colaux, H.; Nishiyama, Y. Resolution Enhancement in Proton Double Quantum Magic-Angle Spinning Spectra by Constant-Time Acquisition. *Solid State Nucl. Magn. Reson.* **2017**, *87*, 104-110.
54. Lesage, A.; Duma, L.; Sakellariou, D.; Emsley, L. Improved Resolution in Proton NMR Spectroscopy of Powdered Solids. *J. Am. Chem. Soc.* **2001**, *123* (24), 5747-5752.
55. Chen, L. L.; Olsen, R. A.; Elliott, D. W.; Boettcher, J. M.; Zhou, D. H. H.; Rienstra, C. M.; Mueller, L. J. Constant-Time Through-Bond ^{13}C Correlation Spectroscopy for Assigning Protein Resonances with Solid-State NMR Spectroscopy. *J. Am. Chem. Soc.* **2006**, *128* (31), 9992-9993.
56. Zhang, R. C.; Ramamoorthy, A. Constant-Time 2D and 3D Through-Bond Correlation NMR Spectroscopy of Solids under 60 kHz MAS. *J. Chem. Phys.* **2016**, *144* (3), 034202.
57. Alderman, D. W.; McGeorge, G.; Hu, J. Z.; Pugmire, R. J.; Grant, D. M. A sensitive, high resolution magic angle turning experiment for measuring chemical shift tensor principal values. *Mol Phys* **1998**, *95* (6), 1113-1126.
58. Chen, L.; Wang, Q. A.; Hu, B. W.; Lafon, O.; Trebosc, J.; Deng, F.; Amoureux, J. P. Measurement of Hetero-Nuclear Distances Using a Symmetry-Based Pulse Sequence in Solid-State NMR. *Phys. Chem. Chem. Phys.* **2010**, *12* (32), 9395-9405.
59. Duong, N. T.; Rossi, F.; Makrinich, M.; Goldbourn, A.; Chierotti, M. R.; Gobetto, R.; Nishiyama, Y. Accurate ^1H - ^{14}N Distance Measurements by Phase-Modulated RESPDOR at Ultra-Fast MAS. *J. Magn. Reson.* **2019**, *308*, 106559.
60. Tosner, Z.; Andersen, R.; Stevens, B.; Eden, M.; Nielsen, N. C.; Vosegaard, T. Computer-Intensive Simulation of Solid-State NMR Experiments using SIMPSON. *J. Magn. Reson.* **2014**, *246*, 79-93.
61. Tosner, Z.; Vosegaard, T.; Kehlet, C.; Khaneja, N.; Glaser, S. J.; Nielsen, N. C. Optimal Control in NMR Spectroscopy: Numerical Implementation in SIMPSON. *J. Magn. Reson.* **2009**, *197* (2), 120-134.
62. Bak, M.; Rasmussen, J. T.; Nielsen, N. C. SIMPSON: A General Simulation Program for Solid-State NMR Spectroscopy. *J. Magn. Reson.* **2000**, *147* (2), 296-330.

63. Ting, V. P.; Schmidtman, M.; Wilson, C. C.; Weller, M. T. Cisplatin: Polymorphism and Structural Insights into an Important Chemotherapeutic Drug. *Angew Chem Int Edit* **2010**, *49* (49), 9408-9411.
64. Kinnun, J. J.; Leftin, A.; Brown, M. F. Solid-State NMR Spectroscopy for the Physical Chemistry Laboratory. *J Chem Educ* **2013**, *90* (1), 123-128.
65. Lee, M.; Goldberg, W. I. Nuclear-Magnetic-Resonance Line Narrowing by a Rotating rf Field. *Phys. Rev.* **1965**, *140* (4a), 1261-1271.
66. Venkatesh, A.; Hung, I.; Boteju, K. C.; Sadow, A. D.; Gor'kov, P. L.; Gan, Z.; Rossini, A. J. Suppressing ¹H Spin Diffusion in Fast MAS Proton Detected Heteronuclear Correlation Solid-State NMR Experiments. *Solid State Nucl. Magn. Reson.* **2020**, *105*, 101636.
67. Harris, R. K.; Becker, E. D.; De Menezes, S. M. C.; Goodfellow, R.; Granger, P. NMR Nomenclature. Nuclear Spin Properties and Conventions for Chemical Shifts - (IUPAC recommendations 2001). *Pure Appl. Chem.* **2001**, *73* (11), 1795-1818.
68. Wang, Q.; Li, Y. X.; Trebosc, J.; Lafon, O.; Xu, J.; Hu, B. W.; Feng, N. D.; Chen, Q.; Amoureux, J. P.; Deng, F. Population transfer HMQC for half-integer quadrupolar nuclei. *J. Chem. Phys.* **2015**, *142* (9), 094201.
69. Brinkmann, A.; Kentgens, A. P. M. Proton-Selective ¹⁷O-¹H Distance Measurements in Fast Magic Angle Spinning Solid-State NMR Spectroscopy for the Determination of Hydrogen Bond Lengths. *J. Am. Chem. Soc.* **2006**, *128* (46), 14758-14759.
70. Oas, T. G.; Griffin, R. G.; Levitt, M. H. Rotary Resonance Recoupling of Dipolar Interactions in Solid-State Nuclear Magnetic-Resonance Spectroscopy. *J. Chem. Phys.* **1988**, *89* (2), 692-695.
71. Levitt, M. H.; Maduh, P. K.; Hughes, C. E. Cogwheel Phase Cycling. *J. Magn. Reson.* **2002**, *155* (2), 300-306.
72. Jerschow, A.; Kumar, R. Calculation of Coherence Pathway Selection and Cogwheel Cycles. *J. Magn. Reson.* **2003**, *160* (1), 59-64.
73. van Meerten, S. G. J.; Franssen, W. M. J.; Kentgens, A. P. M. ssNake: A cross-Platform Open-Source NMR Data Processing and Fitting Application. *J. Magn. Reson.* **2019**, *301*, 56-66.

Supporting Information for:

**Proton-Detected Solid-State NMR Spectroscopy of Spin-1/2 Nuclei with Large
Chemical Shift Anisotropy**

Amrit Venkatesh,^{1,2} Frédéric A. Perras,¹ Aaron J. Rossini^{1,2}*

¹US DOE Ames Laboratory, Ames, Iowa, USA, 50011

²Iowa State University, Department of Chemistry, Ames, IA, USA, 50011

Corresponding Author

*e-mail: arossini@iastate.edu

Table of Contents

Supplementary Information	Page
Figure S1. 2D $^1\text{H}\{^{195}\text{Pt}\}$ CT and AID D-HMQC spectra	S3
Figure S2. 2D $^1\text{H}\{^{35}\text{Cl}\}$ population transfer TONE D-HMQC-3 spectra of histidine	S4
Figure S3. Comparison of ^{35}Cl slices from 2D TONE D-HMQC-3 spectra	S5
Figure S4. Comparison of ^{195}Pt projections of AID D-HMQC spectra	S7
Figure S5. AID TONE D-HMQC-1 pulse sequence and 2D $^1\text{H}\{^{195}\text{Pt}\}$ spectrum	S7
Figure S6. Simulated damped cosine functions to model t_1 -incrementation in AID aMAT D-HMQC	S9
Figure S7. Simulated damped aMAT D-HMQC FIDs to model t_1 -incrementation in AID aMAT D-HMQC	S10
Figure S8. $^1\text{H}\{^{195}\text{Pt}\}$ AID aMAT TONE D-HMQC-2 spectrum (6 min acquisition)	S11
Figure S9. Comparison of CT aMAT (TONE) D-HMQC spectra	S12
Figure S10. SIMPSON simulations of D-HMQC signals for different ^{195}Pt pulses	S13
Table S1. Table showing dipolar couplings and probabilities used in S-REDOR simulations	S6
Table S2. Table summarizing sensitivities of $^1\text{H}\{^{195}\text{Pt}\}$ TONE D-HMQC spectra	S8

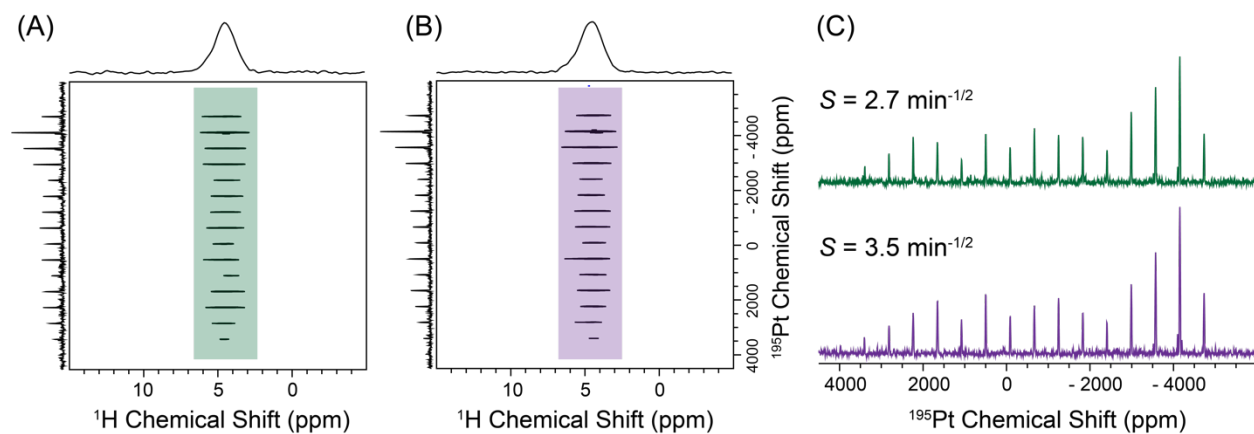


Figure S1. 2D $^1\text{H}\{^{195}\text{Pt}\}$ D-HMQC spectra acquired with (A) CT and (B) AID schemes. (C) Comparison of ^{195}Pt traces from 2D spectra shown in (A) and (B). Sensitivity of the ^{195}Pt traces in (C) is calculated based on the signal-to-noise ratio of the most intense sideband at -4153 ppm. 2D spectra are plotted with the same contour floor level. Spectra were acquired with a 0.9 s recycle delay, 32 scans, an indirect spectral width of 1 MHz and 576 t_1 increments. CT D-HMQC shown in (A) was obtained with $C = 16$, where $C \cdot \tau_r > t_{1,\text{max}}$. States-TPPI was used for quadrature in t_1 .

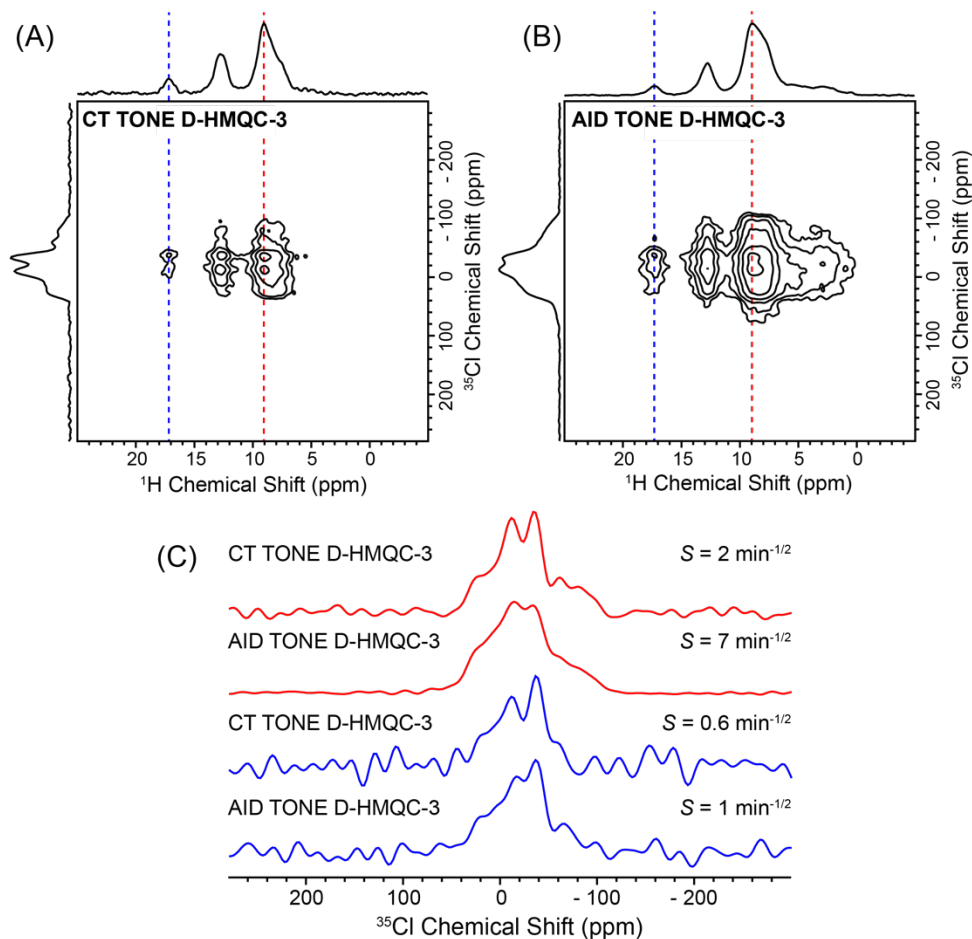


Figure S2. 2D $^1\text{H}\{^{35}\text{Cl}\}$ population transfer (PT) TONE D-HMQC-3 spectra of L-histidine-HCl·H₂O acquired with (A) CT and (B) AID t_1 -incrementation schemes, respectively. (C) Comparison of 1D ^{35}Cl slices extracted from the 2D spectra at ^1H chemical shifts of (red) 9 ppm and (blue) 17.2 ppm. 2D spectra were acquired with a 1 s recycle delay, 8 scans, an indirect spectral width of 200 kHz and 512 t_1 increments. States-TPPI was used for quadrature in t_1 . A 1 ms Lee-Goldburg (LG) spin-lock pulse was applied at 150 kHz rf. The implementation of TONE D-HMQC-3 experiments is described in detail in our previous report (see reference [42] in the main text). The sensitivity of the spectra is indicated in (C).

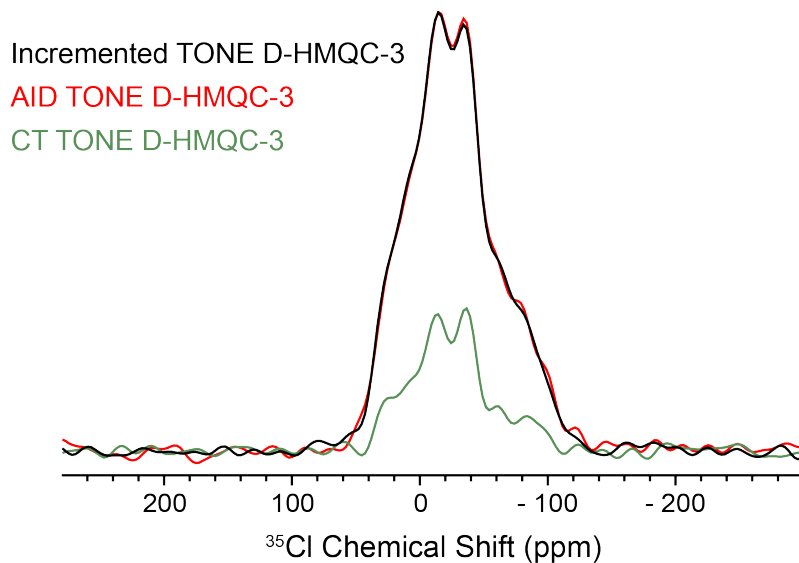


Figure S3. Comparison of 1D ^{35}Cl slices extracted from 2D $^1\text{H}\{^{35}\text{Cl}\}$ PT TONE D-HMQC-3 spectra at a ^1H chemical shift of 9 ppm. The 2D spectra were obtained with a rotor-synchronized t_1 incrementation using (green) CT, (black) standard incremented and (red) AID approaches. Experiments were performed with a 3.9 s recycle delay, 16 scans, an indirect spectral width of 25 kHz and 64 t_1 increments. States-TPPI was used for quadrature in t_1 . A 1 ms Lee-Goldburg (LG) spin-lock pulse was applied at 150 kHz rf. The data clearly shows that AID D-HMQC is equivalent to standard incremented D-HMQC if performed with a rotor-synchronized t_1 incrementation. Although, CT TONE D-HMQC-3 provides the lowest sensitivity, it provides the best resolution.

Table S1. Table showing the dipolar couplings and probabilities used to simulate the $^1\text{H}\{^{195}\text{Pt}\}$ S-REDOR curves of cisplatin shown in Figure 3C.

Dipolar couplings (Hz)	Number of spins (n)	Probability (p_m)	Probability of being nearest (P_m)	Rolling sum of probability
1190*	1	0.338	0.338	0.338
550	1	0.338	0.223756	0.561756
410	1	0.338	0.148126472	0.709882
380	1	0.338	0.098059724	0.807942
240	1	0.338	0.064915538	0.872858
120	1	0.338	0.042974086	0.915832
110	1	0.338	0.028448845	0.944281
100	1	0.338	0.018833135	0.963114
90	1	0.338	0.012467536	0.975581
80	1	0.338	0.008253509	0.983835
70	3	0.709882	0.011475361	0.99531
60	4	0.807942	0.003789083	0.999099
50	3	0.709882	0.000639399	0.999739
40	6	0.915832	0.000239318	0.999978
30	7	0.944281	2.08E-05	0.999999

*Dipolar coupling of 1510 Hz was partially averaged based on the H-Pt-N bond angle of 22° . This results in a scaling of the dipolar coupling by a factor 0.79 ($0.5 \times [3\cos^2 22^\circ - 1]$).

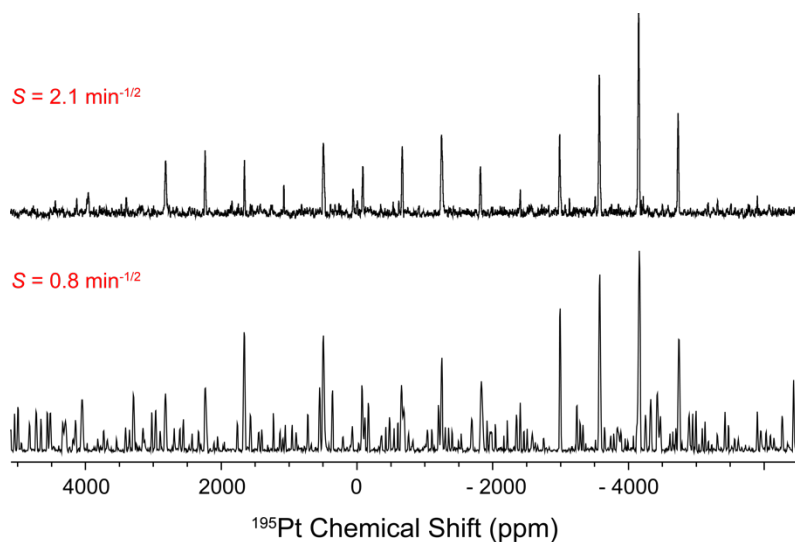


Figure S4. ^{195}Pt projections of 2D $^1\text{H}\{^{195}\text{Pt}\}$ AID D-HMQC spectra shown in (top) Figure 1D and (bottom) Figure 4B of the main text. The MAS frequency was less stable when the spectra shown in Figure 4 were acquired, which resulted in higher t_1 -noise and lower ^{195}Pt sensitivities.

AID TONE D-HMQC-1

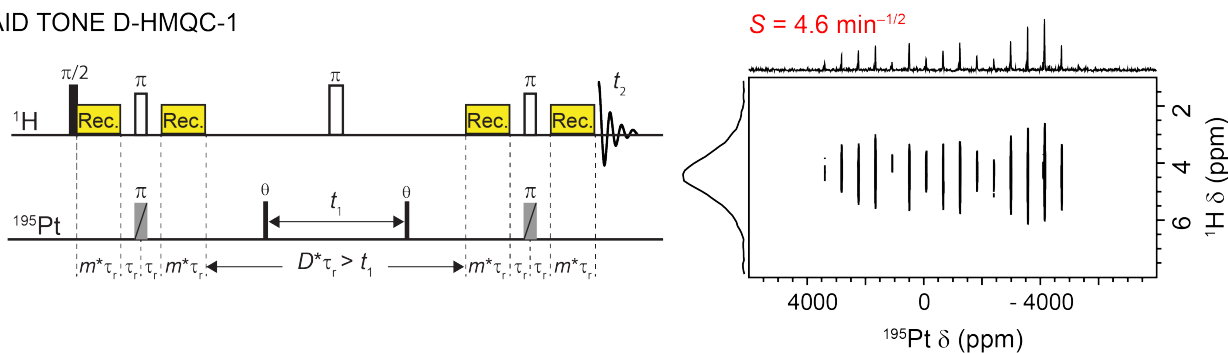


Figure S5. (left) AID TONE D-HMQC-1 pulse sequence and (right) the corresponding 2D $^1\text{H}\{^{195}\text{Pt}\}$ D-HMQC spectrum. The sensitivity of the ^{195}Pt dimension was measured on the positive projection using the most intense sideband and is indicated above the 2D spectrum. Spectrum was acquired with a 1 s recycle delay, 20 scans, an indirect spectral width of 1.25 MHz and 704 t_1 increments. The States scheme was used for quadrature in t_1 .

Table S2. Table summarizing the signal-to-noise ratios and sensitivities of the most intense rows (^1H slice) and columns (^{195}Pt slice) in the 2D spectra shown in Figure 4 and Figure S5.

Experiment	^1H		^{195}Pt		SNR $_{1\text{H}}$ /SNR $_{195\text{Pt}}$
	SNR $_{1\text{H}}$	Sensitivity (min $^{-1/2}$)	SNR $_{195\text{Pt}}$ ^a	Sensitivity (min $^{-1/2}$)	
AID D-HMQC	31	2.3	5	0.4	6.2
AID TONE D-HMQC-1	26	1.7	16	1.0	1.625
AID TONE D-HMQC-2	32	2.1	32	2.1	1.0
AID TONE D-HMQC-4	28	1.8	26	1.7	1.08
AID TONE D-HMQC-5	28	1.8	28	1.8	1.0

^aThe ^{195}Pt SNR was measured with the most intense sideband in the manifold.

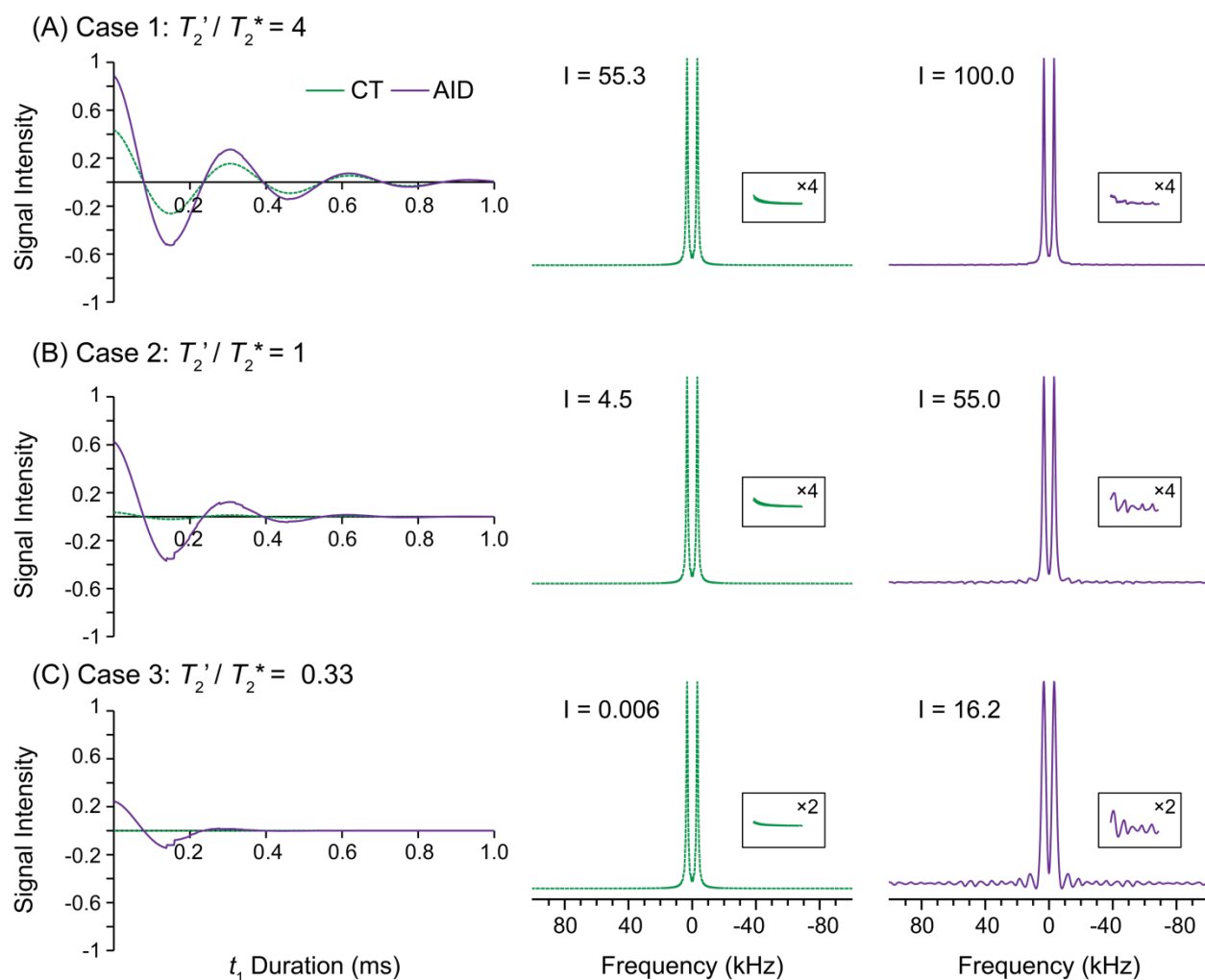


Figure S6. (A-C, left) Simulated damped cosine functions to model the t_1 -incrementation and sensitivity losses due to homogeneous ^1H transverse relaxation (T_2') for CT aMAT D-HMQC (green, dashed line) and AID aMAT D-HMQC (purple, solid line). The inhomogeneous transverse relaxation time constant (T_2^*) of the indirect detected spin was fixed at 0.3 ms. The ratio of T_2' / T_2^* was (A) 4, (B) 1 and (C) 0.33. Note that the aMAT sequences employ a minimum ^1H echo duration of 7 rotor periods and that the number of rotor periods cannot be a multiple of 3 (see reference no. 40 in the main text). Spectra obtained from Fourier transformation of the corresponding cosine functions are shown for (center) CT aMAT D-HMQC and (right) AID aMAT D-HMQC. The peak intensities of the frequency spectra are normalized with respect to AID D-HMQC in case 1 (purple trace on top-right).

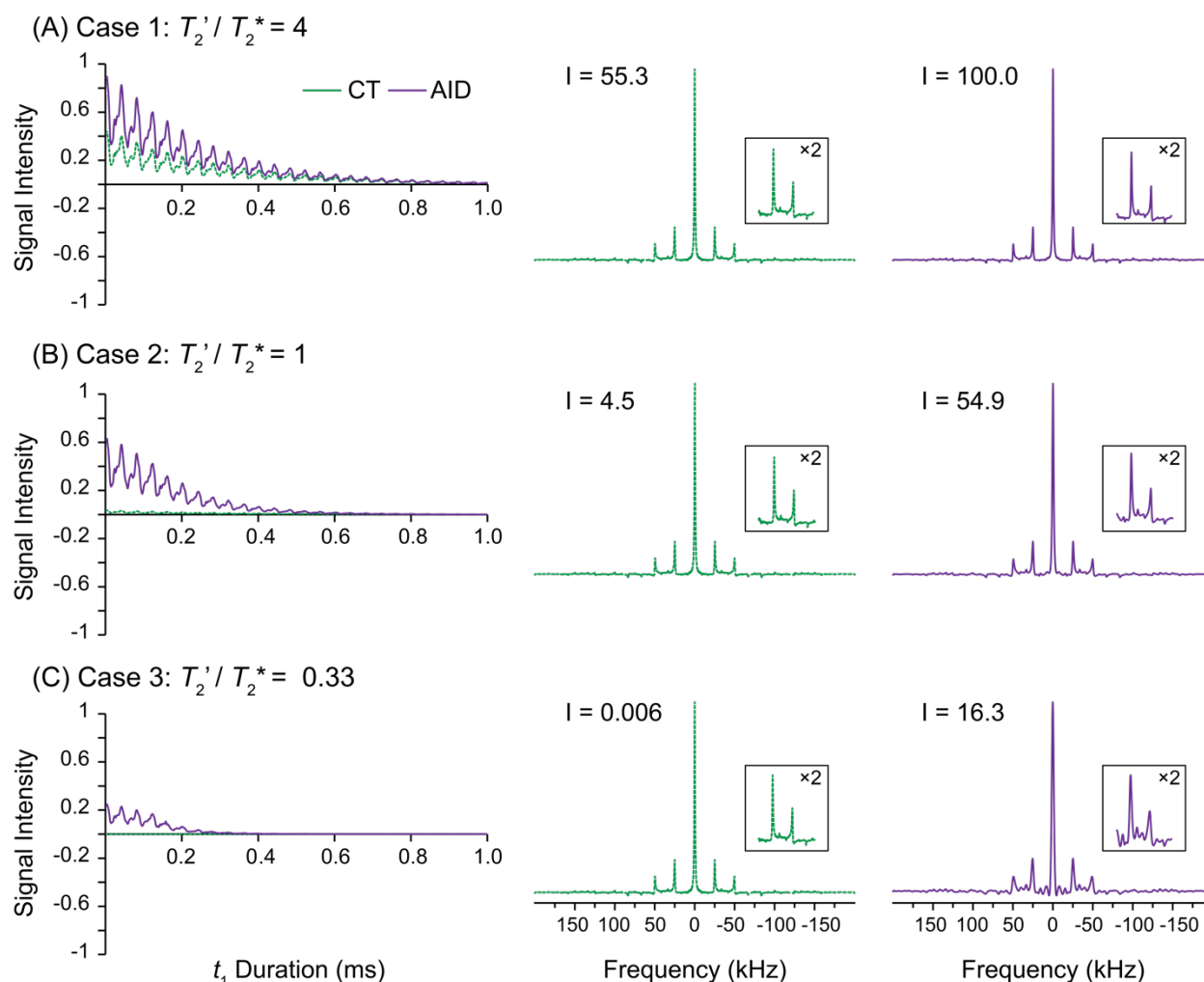


Figure S7. (A-C, left) Simulated damped aMAT D-HMQC FIDs to model the t_1 -incrementation and sensitivity losses due to homogeneous ^1H transverse relaxation (T_2') for CT aMAT D-HMQC (green, dashed line) and AID aMAT D-HMQC (purple, solid line). The aMAT D-HMQC FID was simulated using SIMPSON using the same Tanh/Tan shape, pulse lengths and powers as the experiments. The inhomogeneous transverse relaxation time constant (T_2^*) of the indirect detected spin was fixed at 0.3 ms. The ratio of T_2'/T_2^* was (A) 4, (B) 1 and (C) 0.33. Note that the aMAT sequences employ a minimum ^1H echo duration of 7 rotor periods and that the number of rotor periods cannot be a multiple of 3 (see reference [40] in the main text). Spectra obtained from Fourier transformation of the corresponding aMAT D-HMQC FIDs are shown for (center) CT aMAT D-HMQC and (right) AID aMAT D-HMQC. Similar to the experiments, residual spinning sidebands (at integer multiples of $\pm 0.5\nu_r$) are observed beside the most intense isotropic signal due to the relatively long duration of the SHAP pulses (see reference [40] in the main text). The peak intensities of the frequency spectra are normalized with respect to AID D-HMQC in case 1 (purple trace on top-right).

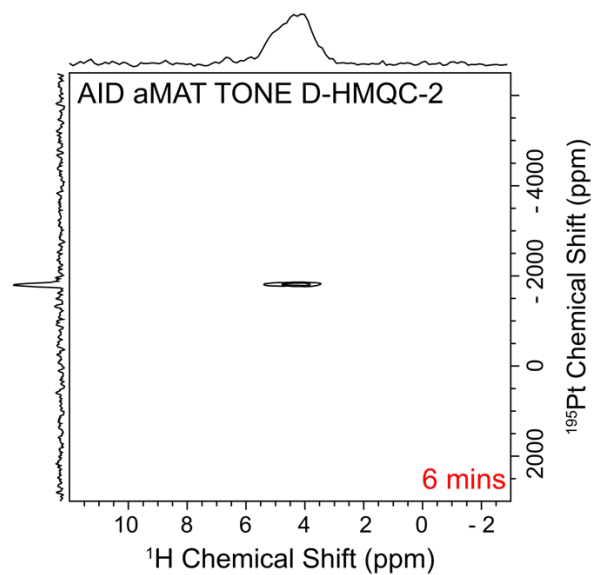


Figure S8. $^1\text{H}\{^{195}\text{Pt}\}$ AID aMAT TONE D-HMQC-2 spectrum of cisplatin obtained in 6 minutes. The spectrum was acquired with a 1 s recycle delay, 2 scans, an indirect spectral width of 1.25 MHz and 182 t_1 increments. The States scheme was used for quadrature in t_1 .

Constant-time experiments

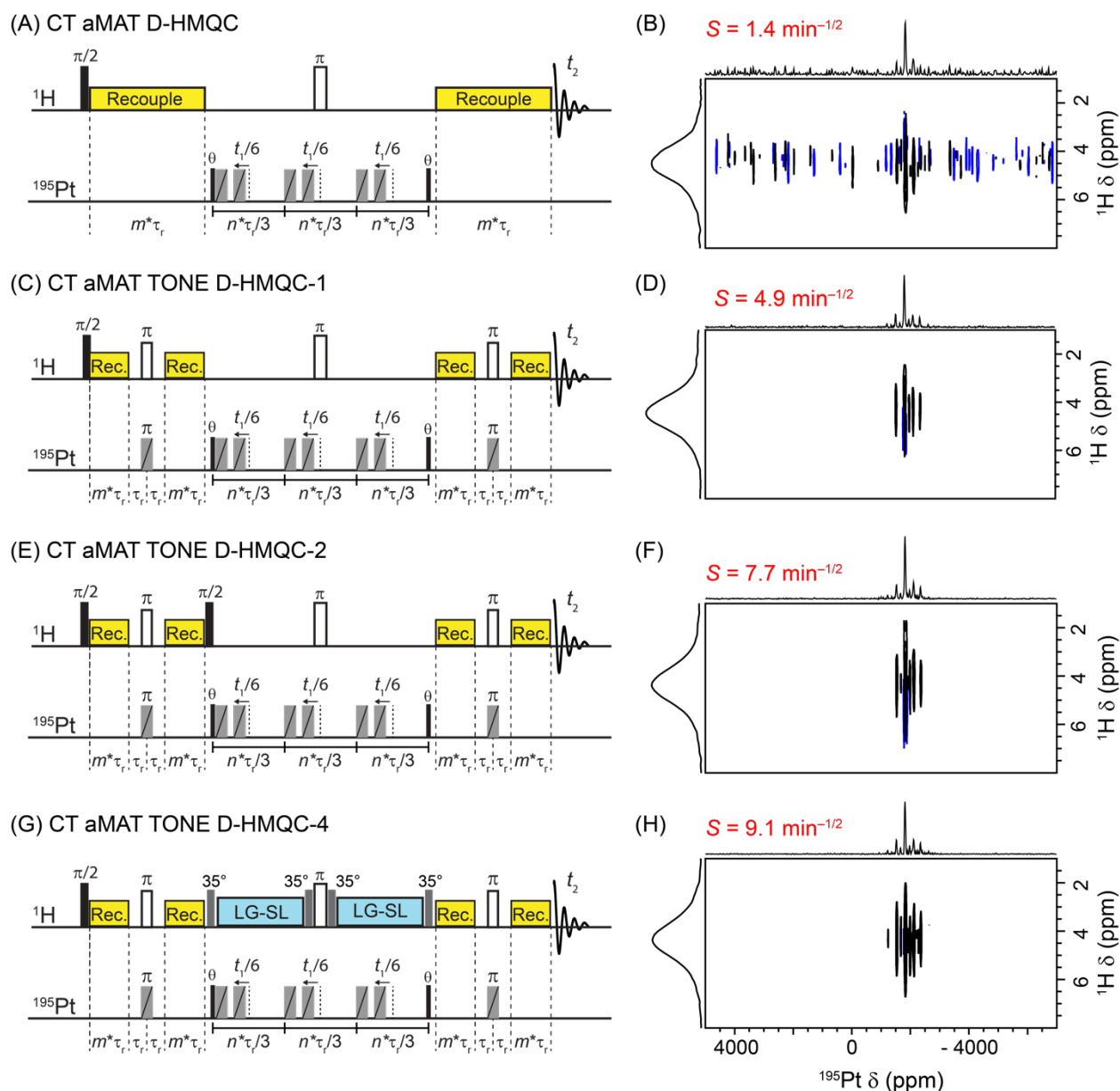


Figure S9. (A) CT aMAT D-HMQC, (C) CT aMAT TONE D-HMQC-1, (E) CT aMAT TONE D-HMQC-2 and (G) CT aMAT TONE D-HMQC-4 pulse sequences and (B, D, F, H) the corresponding 2D $^1\text{H}\{^{195}\text{Pt}\}$ D-HMQC spectra of cisplatin. The sensitivity of the ^{195}Pt dimension was measured on the positive projection and is indicated above each 2D spectrum. The spectrum was acquired with a 1 s recycle delay, 98 scans, an indirect spectral width of 1.25 MHz and 392 t_1 increments. The States scheme was used for quadrature in t_1 .

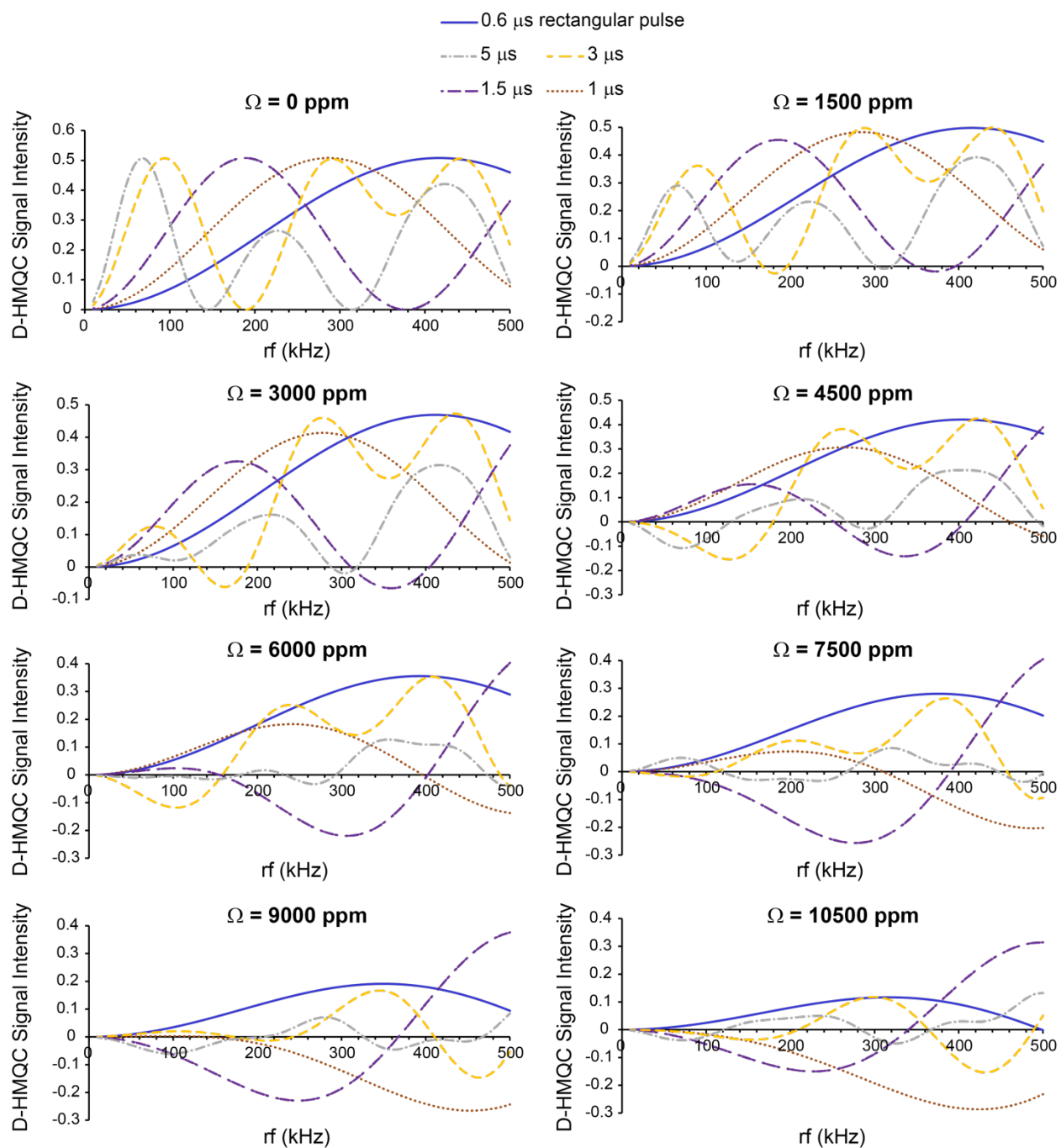


Figure S10. Plots showing the SIMPSON simulated variation of $^1\text{H}\{^{195}\text{Pt}\}$ D-HMQC signal intensity with rf field for different ^{195}Pt excitation pulses (0.6 μs rectangular pulse, and 5, 3, 1.5 and 1 μs SHAPs), at different ^{195}Pt Ω values (indicated above each plot). The ^{195}Pt κ was set to -1 in all cases. The sweep widths of the SHAPs were either 5 MHz (for 5 μs SHAP) or 3 MHz (for 3, 1.5 and 1 μs SHAP). Simulations used the rep168 crystal file with 17 gamma angles.